Technique and Application of a Non-Invasive Three Dimensional Image Matching Method for the Study of Total Shoulder Arthroplasty

by

Daniel Frank Massimini

B.S., Mechanical Engineering
University of California at Los Angeles (UCLA), 2005

Submitted to the Department of Mechanical Engineering
in Partial Fulfillment of the Requirements for the Degree of
Master of Science in Mechanical Engineering

at the

Massachusetts Institute of Technology

February 2009

Signature of Author .....
Department of Mechanical Engineering
December 19, 2008

Certified by .....
Guoan Li, PhD
Associate Professor of Orthopaedic Surgery
Harvard Medical School
Thesis Supervisor

Certified by .....
Derek Rowell, PhD
Professor of Mechanical Engineering
Thesis Supervisor

Accepted by .....
David E. Hardt, PhD
Professor of Mechanical Engineering
Chairman, Department Committee on Graduate Students

Technique and Application of a Non-Invasive Three Dimensional Image Matching Method for the Study of Total Shoulder Arthroplasty

by

Daniel Frank Massimini

Submitted to the Department of Mechanical Engineering
on December 19, 2008 in Partial Fulfillment of the
Requirements for the Degree of
Master of Science in Mechanical Engineering

Abstract

Knowledge of in-vivo glenohumeral joint biomechanics after total shoulder arthroplasty are important for the improvement of patient function, implant longevity and surgical technique. No data has been published on the in-vivo glenohumeral joint contact locations in patients after total shoulder arthroplasty. Therefore, the objectives of this thesis were to determine the in-vivo glenohumeral joint contact locations and humeral head translations in patients after total shoulder arthroplasty.

First, a non-invasive three dimensional fluoroscopic image matching method was developed and validated for use in the shoulder joint complex. Next, a group of patients that have undergone clinically successful total shoulder arthroplasty surgeries were recruited for study and imaged by the fluoroscopic imaging technique. The fluoroscopic imaging system was recreated in a virtual environment and the in-vivo kinematics that were recorded by the fluoroscopes were recreated with three dimensional models. The contact centroids of the glenohumeral joint and humeral head translations were measured using solid modeling software.

In summary, this thesis quantified the in-vivo glenohumeral joint contact locations and humeral head translations after total shoulder arthroplasty. These data provides surgeons and engineers valuable information for developing surgical treatments that may better help recreate ‘normal’ motion of the shoulder after total shoulder arthroplasty.

Thesis Supervisor: Guoan Li, PhD

Title: Associate Professor of Orthopaedic Surgery
Harvard Medical School

Acknowledgements

As I look back on the last three years of my life that I have lived in Boston, I often wonder where all my time has gone. There is so much to see and do in this city, yet I feel that I have seen and done so little. As I begin my fourth year at MIT, I realize that I will never get to be a tourist in the city that I now call home. Life just continues to snowball faster and faster at an unprecedented velocity that I never imagined possible. Although this is not to say that I haven't thoroughly enjoyed my time as a graduate student at MIT, albeit filled with many ups and downs along the way. Yet looking back, I would not have done anything differently. In between juggling classes, research, president of Snowriders (06-07), organizing two graduate student ski trips (07 & 08), getting food for various G.A.M.E events, making new friends and living life to the fullest, I would say that I have had my hands full. However, without the following (truncated list due to space limitations, although not forgotten) people in my life, my journey at MIT thus far would not have been possible.

First, I must thank God for making this whole reality possible, for every detail that He planned for my existence and for the amazing abilities that I was given. Next, I would like to thank my adviser Dr. Guoan Li, for always believing in my abilities, for standing up for me, for his patience and for being a mentor and a friend. Without his belief and the support of his MGH Bioengineering Lab, I would not have had this amazing opportunity. To Dr. Jon Warner, for all his clinical insight of the shoulder joint complex and for making my research possible. To Dr. Derek Rowell for advising my academic choices at MIT and for always confusing me with some guy named

Mike. I am glad we can both laugh about it. Additionally, I would like to thank each and every member of the MGH Bioengineering Lab both past and present for his or her contribution to my life. I would also like to thank Leslie Regan and Joan Kravit in the Mechanical Engineering Graduate Office and Laurie Ward for all her help making Snowriders so successful.

Also, I thank my family for understanding my decision to uproot and move across the country from sunny southern California to snowy cold Boston to pursue a graduate degree from MIT. Boston isn't that cold after all. To my Dad for not getting too angry when I drilled holes (age: three) in his shop floor and for not putting tools back (age: current) in their assigned location. To my Mom for sending me care packages of soap, toothpaste and dental floss because for some strange reason these items are not available on the East Coast. To my sister Leanna and brother Joseph for maintaining an incredibly close relationship even though we are so far away. To all my aunts, uncles, cousins, relatives and grandparents, I thank you so much for caring and loving me.

Finally, I thank Sarah for dragging me to the library on weekends to compose this thesis. For all her understanding, patience and ability to motivate, I am forever grateful. I cherish the time we have spent together and look forward to the time I hope to share.

With humbleness and gratitude,

~Daniel

Contents

List of Figures

List of Tables

Chapter 1

1.1 Introduction

Total shoulder arthroplasty (TSA) has become a popular clinical choice for the treatment of end-stage shoulder degeneration for a restoration of range-of-motion (ROM) and pain relief[1]. The term arthroplasty refers to the surgical removal and replacement of degenerative articular cartilage surfaces with engineered materials to substitute for the body's natural joint structures. Current TSA involves the surgical visualization of the humeral head and glenoid articular surface in order to remove the damaged structures with a bone saw and be replaced with a polyethylene glenoid component and cobalt chromium humeral head. Dr. Charles Neer II first pioneered this technique in 1953, when he created the first 'monoblock' design at the Columbia-Presbyterian Medical Center at Columbia University[2]. Since that time, numerous component designs and surgical techniques have been introduced to the market, each with varying degrees of clinical success and acceptance. Surgical techniques have evolved from simply making due with the implants available to careful balancing of soft tissues around the anatomic components with minimally invasive surgeries. The wide variety of available shoulder implant designs has primarily focused on material selection, fixation features, anatomic sizing and most recently recreation of the anatomic geometry of the healthy glenohumeral joint. Needless to say, these advancements are only as capable as the surgeon performing the operation. Numerous component failures such as component loosening and polyethylene damage have been reported after implantation[3-7]. Several current case studies[3, 8, 9]

have sought to correlate complication rates, range of motion, subjective shoulder values (SSV) and pain scores with surgical technique, rehabilitation protocol and the number of TSA operations performed by a surgeon per year. However, the quantitative factors that influence these patient outcomes and affect the performance of TSA in-vivo are fairly limited. No data has been reported on the glenohumeral joint articular contact locations or humeral head translations in patients following TSA. Such contact kinematic data are necessary for the improvement of implant designs and surgical implantation technique; and ultimately to enhance component longevity. Therefore, the purpose of this research was to validate a non-invasive imaging technique and investigate the glenohumeral articular contact locations and humeral head translations after anatomic TSA during active in-vivo shoulder abduction with neutral, internal and external rotations using a novel dual plane fluoroscopic image matching technique.

1.2 Shoulder Overview

The shoulder joint complex has the greatest ROM and is the least constrained joint within the human body. It is comprised of four separate joints, the acromioclavicular, the sternoclavicular, the scapulothoracic, and the glenohumeral joint (Fig 1). The two primary joints that contribute to the ROM and stability of the

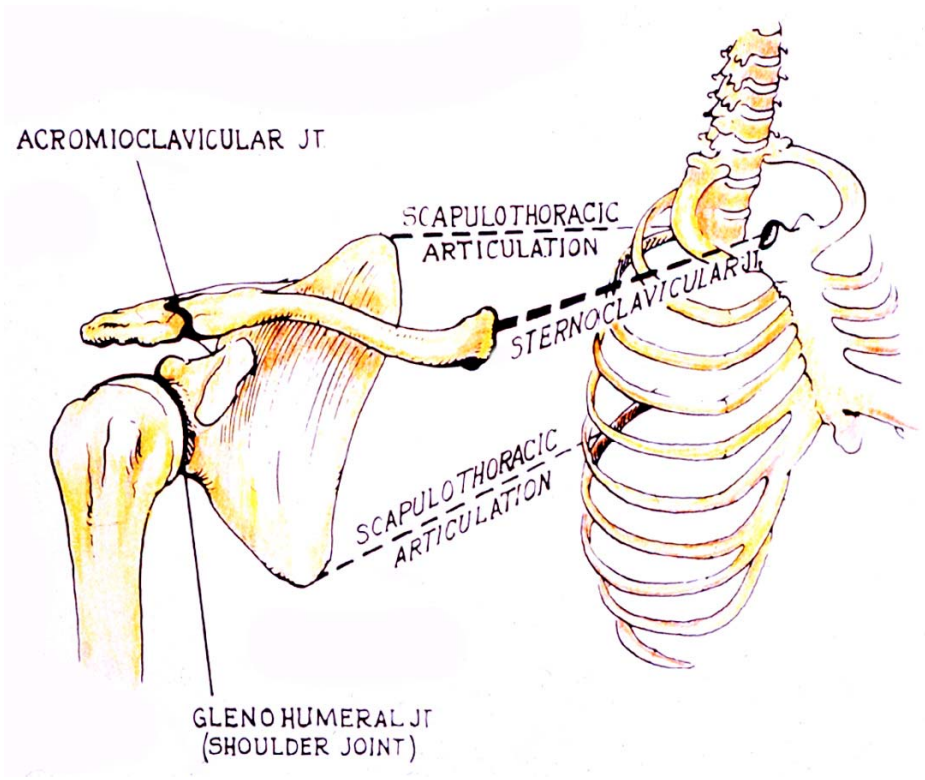

Figure 1 The intercalated joints of the shoulder complex.

shoulder joint complex are the scapulothoracic and the glenohumeral joints. The scapulothoracic joint is the tethering of the scapula to the thoracic rib cage by the serratus anterior muscle and interdigitated fascia. The smooth gliding motion of the scapula bone on the thoracic ribs results from contraction and relaxation of the serratus anterior muscle and the elasticity of interdigitated fascia sandwiched

between the bones. On the other hand, the glenohumeral joint is a diarthrodial joint where opposing bone surfaces of the glenoid and humeral head are covered in

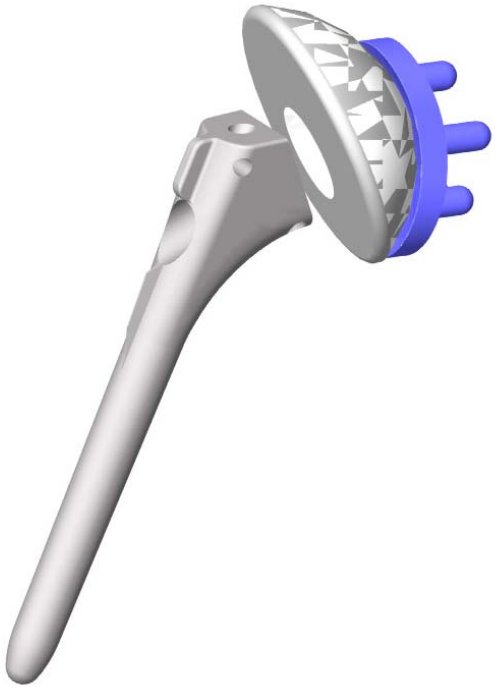

Figure 2 Typical total shoulder arthroplasty components.

hyaline articular cartilage such that the bones of the scapula and humerus directly interact with one another transmitting forces through the cartilage layer. Osteoarthritis (OA) is the progressive degenerative breakdown of the hyaline articular cartilage within a joint that causes bone-on-bone contact. This bone-on-bone contact is incredibly painful and causes many individuals to minimize their use of the affected joint, such that, in extreme cases the pain is so severe that the individual cannot use the joint at all. In these extreme cases a total joint replacement (arthroplasty) may help restore range-of-motion and relieve pain. Dr. Charles Neer II pioneered total shoulder arthroplasty in 1953, when he created the first 'monoblock' design at the Columbia-Presbyterian Medical Center at Columbia University[2].

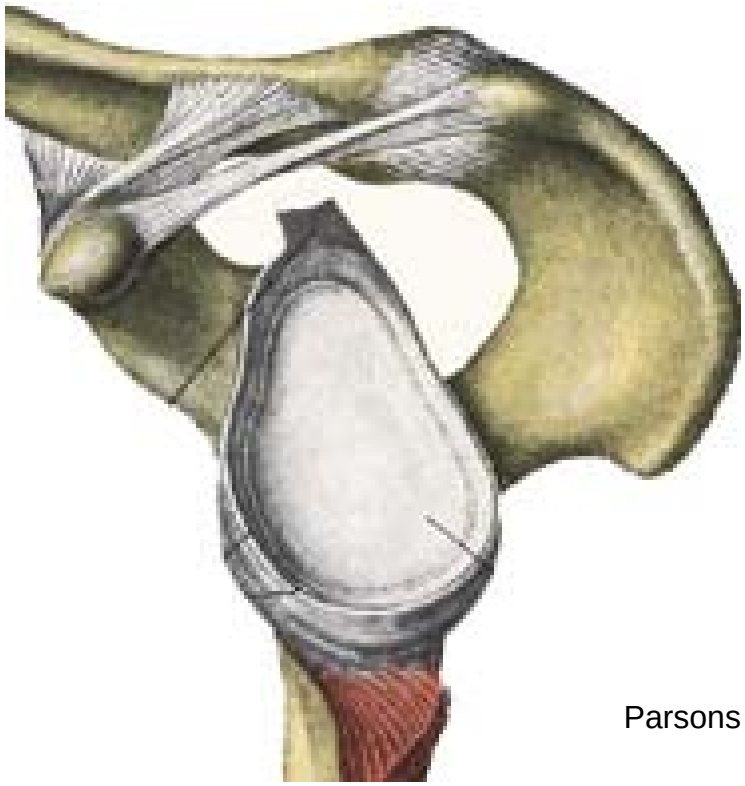

Figure 3 Natural articular surface of the glenoid.

Total shoulder arthroplasty consists of replacing the native articular cartilage of the glenoid and the humeral head with a polyethylene glenoid component and polished cobalt chromium humeral head component (Fig 2). The glenoid component is made from ultra high molecular weight polyethylene and is shaped to mimic the natural glenoid (Fig 3). The natural glenoid excluding the labrum is on average 39±3.7mm (30-48mm) in the superior-inferior direction, 23±2.7mm (18-30mm) in the anterior-posterior direction in the superior half and 29±3.1mm (21-35mm) in the anterior-posterior direction in the inferior half of the glenoid[10] (Fig 4). The articular area[11] (Parsons I.M IV 1998 Lecture Presentation Notes, University of Pittsburgh) is 800-850 mm^2 with an average articular radius[10-12] of curvature of 27.2 ±1.6mm and a bony radius of curvature of 33.4±3.4mm. The humeral head component is made

from polished cobalt chromium and is spherically shaped like the natural humeral head that has a uniform layer of articular cartilage. The articular surface area of the humeral head is approximately three times greater than the articular surface area of the glenoid. The radius of bony curvature[10-12] of the humeral head is on average 25.2±0.7mm and the radius of articular curvature is 25.5±1.5mm (Fig 5). The smaller radius of curvature of the humeral head to that of the glenoid is defined as the radial mismatch and is important for allowing the humeral head to translate and rotate on the glenoid articular surface[4, 5, 13].

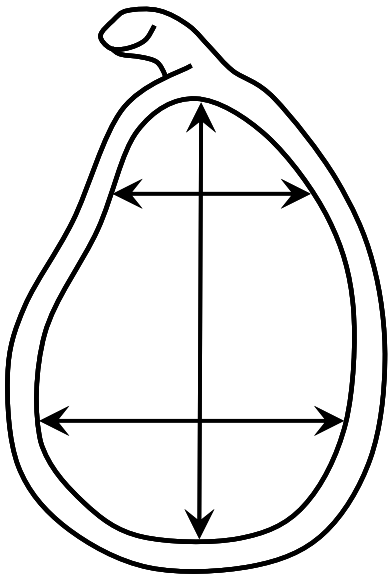

Figure 4 Glenoid surface.

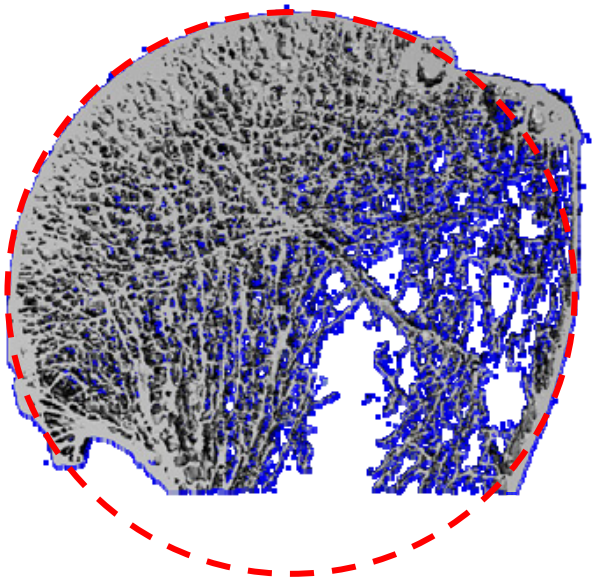

Figure 5 Humeral head radius of curvature.

The stability of the shoulder joint is a compromise between static and dynamic restraints[14, 15]. The static restraints being the superior glenohumeral ligament, the medial glenohumeral ligament, the anterior and posterior bands of the inferior glenohumeral ligament, the axillary pouch of the inferior glenohumeral ligament, the posterior capsule, the biceps tendon, the labrum and the articular cartilage (Fig 6).

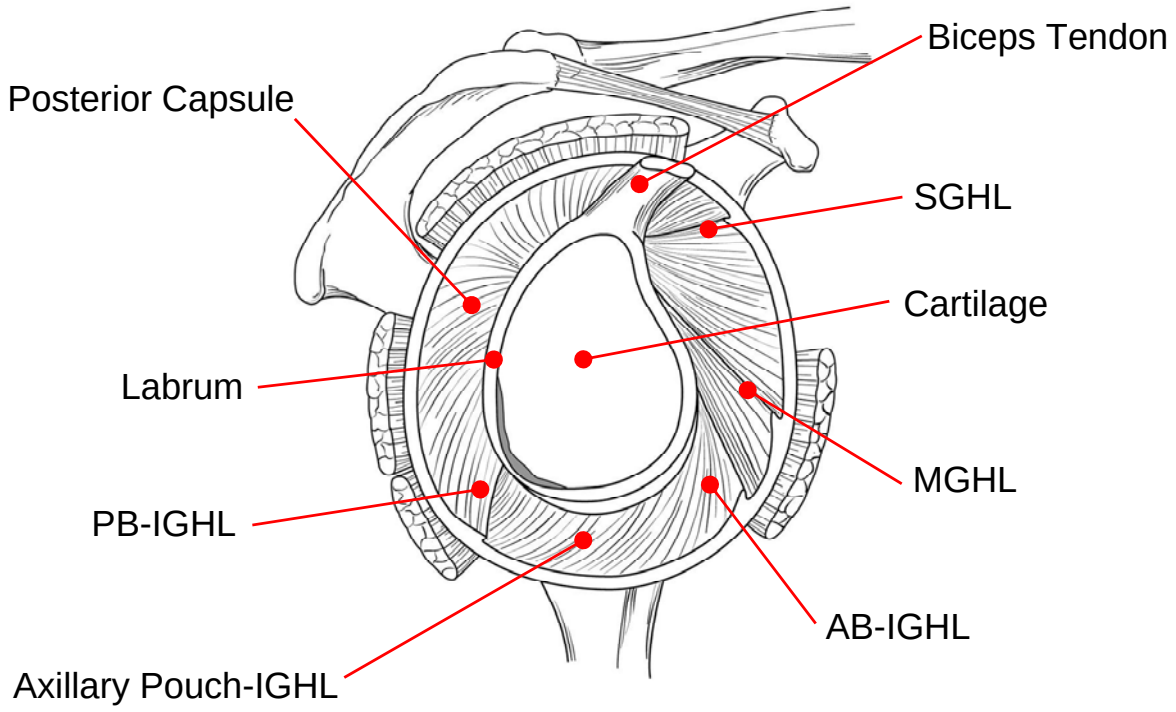

Figure 6 Static restraints of the shoulder joint complex.

The function of the ligaments is to limit excess translation and rotation of the humeral head on the glenoid surface at the extreme ranges of motion[14, 16]. The dynamic restraints are the muscles of the rotator cuff, which are the infraspinatus, supraspinatus, subscapularis and teres minor (Fig 7). Together the combined forces generated by these muscles compress the humeral head into the glenoid cavity creating a compressive stabilizing effect[14, 17]. Damage to these muscles can severely limit the function and stability of the shoulder joint. In the healthy shoulder, proper balance between agonist and antagonist rotator cuff muscles provide dynamic stability, such that in a total shoulder replacement surgery, the surgeon must properly tension these muscles after resecting their insertions to implant the components.

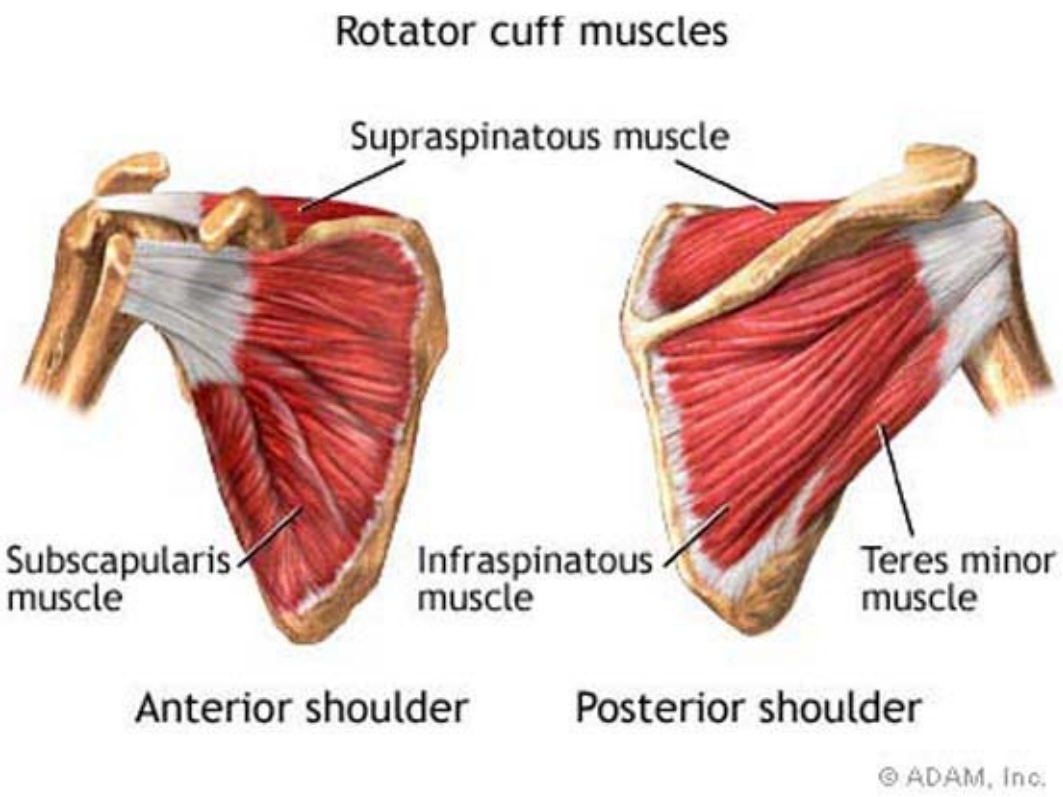

Figure 7 The muscles of the rotator cuff.

Thus a successful total shoulder arthroplasty operation serves not only to reduce pain by replacing the damaged articular cartilage surfaces with engineered implants, but helps restores ROM by restoring balance to the rotator cuff muscles that degenerate over time.

1.3 Previous Research

Prior knowledge of TSA can be categorized as retrospective clinical reports, in-vitro laboratory experiments, computational studies and in-vivo patient analysis. Each of these research designs are not without their advantages and limitations, first and foremost, in-vivo patient analysis is the only method to capture data with functional muscle loads. Clinical reports have shown component failure, such as glenoid component loosening and polyethylene damage after implantation[3-7]. Several current case studies[3, 8, 9] have sought to correlate complication rates, range of motion, subjective shoulder values (SSV) and pain scores with surgical technique, rehabilitation protocol and the number of TSA operations performed by a surgeon per year. In-vitro cadaveric experiments[16-23], albeit limited in muscle loading schemes, have isolated geometric and soft tissue factors that affect the amount of translation and rotation of the humeral head relative to the glenoid surface. These in-vitro studies have reveled that a wide range of normal glenohumeral translations [12, 17, 19, 23-28] could exist in the healthy population. Computational finite element[13, 29, 30], radiographic [4, 31] and laboratory [5, 32, 33] studies have highlighted the importance of glenohumeral radial mismatch on glenoid loosening. Finite element and laboratory studies have also provided theoretical values for TSA glenohumeral translations and force transmission into the glenoid surface[6, 13, 29, 30, 32, 34, 35]. Glenoid retrieval studies have helped to create a classification system for damage mechanisms of the polyethylene component while identifying locations on the glenoid surface that experience a greater degree of damage in-vivo[6, 7, 36, 37]. Bergmann et al. have

developed an instrumented shoulder prosthesis[38] to measure the in-vivo dynamic loads, but not location, experienced by the glenohumeral joint during functional activities such as combing ones hair. The in-vivo translations of the center of the humeral head relative to the glenoid fossa have been reported using several techniques[26, 31, 39-41]. However, no data has been reported on the glenohumeral joint articular contact locations and humeral head translations in patients following TSA.

1.4 Conclusion - Why This Research Was Done

Total shoulder arthroplasty has become the gold standard for restoring ROM and pain relief in degenerative shoulder disease. However, accurate knowledge of in-vivo shoulder kinematics still eludes orthopaedists and researchers. Accurate in-vivo kinematics is the foundation for relative motion between bones, contact patterns of articular surfaces and boundary conditions for finite element and inverse dynamic studies. These data provide orthopaedists and bioengineers a quantitative assessment of normal shoulder motion and the tools which to understand the efficacy that various surgical modalities have on restoring shoulder pathologies. To date, no data has been reported on the glenohumeral joint articular contact locations or humeral head translations in patients following TSA. Contact locations in patients following TSA could be compared to healthy shoulders to determine if normal contact kinematics are restored following surgical reconstruction. Such contact kinematic data are necessary for the improvement of implant designs and surgical implantation technique; and ultimately to enhance component longevity. These data combined with humeral head translations provide in-vivo parameters for wear simulators of the polyethylene glenoid component and a basis which to compare damage modes of failed glenoid components. Thus, quantitatively measuring in-vivo shoulder kinematics would open new doors in the field of shoulder biomechanics. Therefore, the purpose of this research was to investigate the glenohumeral articular contact locations and humeral head translations after anatomic TSA during dynamically stabilized in-vivo shoulder abduction with neutral, internal and external rotations using a novel dual plane fluoroscopic imaging technique.

1.5 Related Publication & Conferences

Manuscripts

1. “Glenohumeral Contact Kinematics In Patients After Total Shoulder Arthroplasty” Daniel F Massimini, Jon JP Warner, Guoan Li (Submitted to JBJS: American)

2. “Humeral Head Translations: Greater Than Previously Thought – A Study in Total Shoulder Arthroplasty” Daniel F Massimini, Jon JP Warner, Guoan Li (Draft in Progress)

Posters, Abstracts & Talks

1. “Patient Specific In-Vivo Shoulder Contact Kinematics After Total Shoulder Arthroplasty” Massimini DF, Li G, Warner JP (53rd ORS Annual Meeting 2007, Poster and Podium)

2. “Validation of a Non-Invasive Measurement of Glenohumeral Articular Surface Contact After TSA Utilizing a Silicon Rubber Technique” Massimini DF, Li G, Warner JP (54th ORS Annual Meeting 2008, Poster)

3. “Glenohumeral Articular Contact Kinematics of Patients After Total Shoulder Arthroplasty” Massimini DF, Li G, Warner JP (54th ORS Annual Meeting 2008, Poster)

4. “Dynamic Scapular Motions of the Shoulder After Total Shoulder Arthroplasty Using an Imaging Technique” Massimini DF, Li G, Warner JP (54th ORS Annual Meeting 2008, Poster)

5. “Dynamic In-Vivo Scapular Motion in Abduction and Adduction” Massimini DF, Warner JP, Li G (ASME Summer Biomechanics Conference, June 2008, Poster)

6. “In-Vivo Shoulder Contact Kinematics After Anatomic Total Shoulder Arthroplasty” Massimini DF, Li G, Warner JP (76th AAOS Annual Meeting 2009, Podium)

Chapter 2

2.1 Non-Invasive Image Matching Method

The concept of image matching is relatively straightforward. A 2D planer image or picture of an object is taken and the spatial 3D orientation of the object is recreated or matched by viewing the object from the perspective of the camera to the image plane and adjusting its position until the projected silhouette overlaps the object's contours on the planer image. By matching multiple objects in the image plane, it is possible to determine the relative position of the objects in spatial coordinates. This technique assumes the knowledge of the distance between the camera and image plane and the acquisition of accurate 3D models of the objects in question. Accurate models may be obtained by coordinate measuring machines (CMM), laser scanning tools, advanced medical imaging techniques such as MRI and CT and directly from Computer Aided Design (CAD) drawings. However, the single image plane method described above suffers from out-of-plane accuracy, which is the inability to determine the true distance of the object from the image plane, but can be improved upon by using two simultaneous image planes. In essence, the second image plane's in-plane accuracy becomes the out-of-plane accuracy of the first image plane.

Thus, this dual plane image matching technique lends itself to studying the bones and implants within the human body to analyze the kinematics of various

joints. However, to look at the bones and implants within the human body, x-rays or fluoroscopic images need to be used in place of standard photographs. First, a joint of interest is positioned within the field-of-view of two fluoroscopes of known orientation and simultaneous images are taken of the desired joint pose. Next, the fluoroscopic images are corrected for geometric distortion. Then a virtual dual plane fluoroscopic imaging system is created in computer space based on the known orientation of the fluoroscopes during imaging. Three-dimensional models of the subject's bones or implants are imported into the virtual environment and matched to 2D features on the acquired image pairs. From each matched pose, the joint kinematics has been accurately recreated and the relative position of the bones or implants can be quantitatively described. Therefore, this dual plane imaging matching technique with its non-invasive and accurate nature can be safely applied to study the kinematics of the shoulder joint complex after total shoulder arthroplasty.

2.2 Dual [plane] Fluoroscopic Imaging System (DFIS)

The dual plane fluoroscopic imaging system [DFIS] consists of two standard mobile C-arm fluoroscopes (12" BV Pulsera, Phillips, USA) arranged with the image intensifiers slightly skewed from orthogonal to create an imaging volume such that the human shoulder does not contact either imaging plane during normal motion. Each C-arm is outfitted with a 12 inch diameter image intensifier such that the combined imaging volume is approximately 30 x 30 x 30 cm^3. This imaging volume creates a field-of-view that captures the scapula and proximal humerus bones throughout their normal range of motion such that the system is capable of capturing the kinematics of the glenohumeral joint during functional daily activities (Fig 8).

Figure 8 Dual plane fluoroscopic imaging system shown with a subject in the central viewing volume with the shoulder in 90° abduction with maximum external rotation.

The distance between the radiation source and the fluoroscopic image intensifier is approximately 96 cm providing ample room for the subject to freely maneuver within. The fluoroscopes, in addition to static image capture, have the capability to record 30, 15 and 8 images per second at a uniform distribution. This cinematic image recording capability allows the DFIS to capture dynamic joint motion in real-time. A custom switch unit was built to operate both fluoroscopes simultaneously such that the image pairs recorded are synchronized in time (Fig 9).

Figure 9 Custom switch unit built to operate two fluoroscopes simultaneously with a single input from the operator. Red and black buttons toggle high and low radiation dosage, respectively.

During each data collection trial, calibration images are taken of radio-opaque ball bearings (beads) in a known orientation for creation of the virtual DFIS environment

and of a copper grid for image distortion correction. The fluoroscopes electronically record the images with 1024 x 1024 pixel resolution in DICOM file format in 8-bit grayscale, corresponding to an actual field-of-view that is 295 x 295 mm (Fig 10). For data analysis, the images are offloaded from the fluoroscopes to a personal computer and RAID backup storage system.

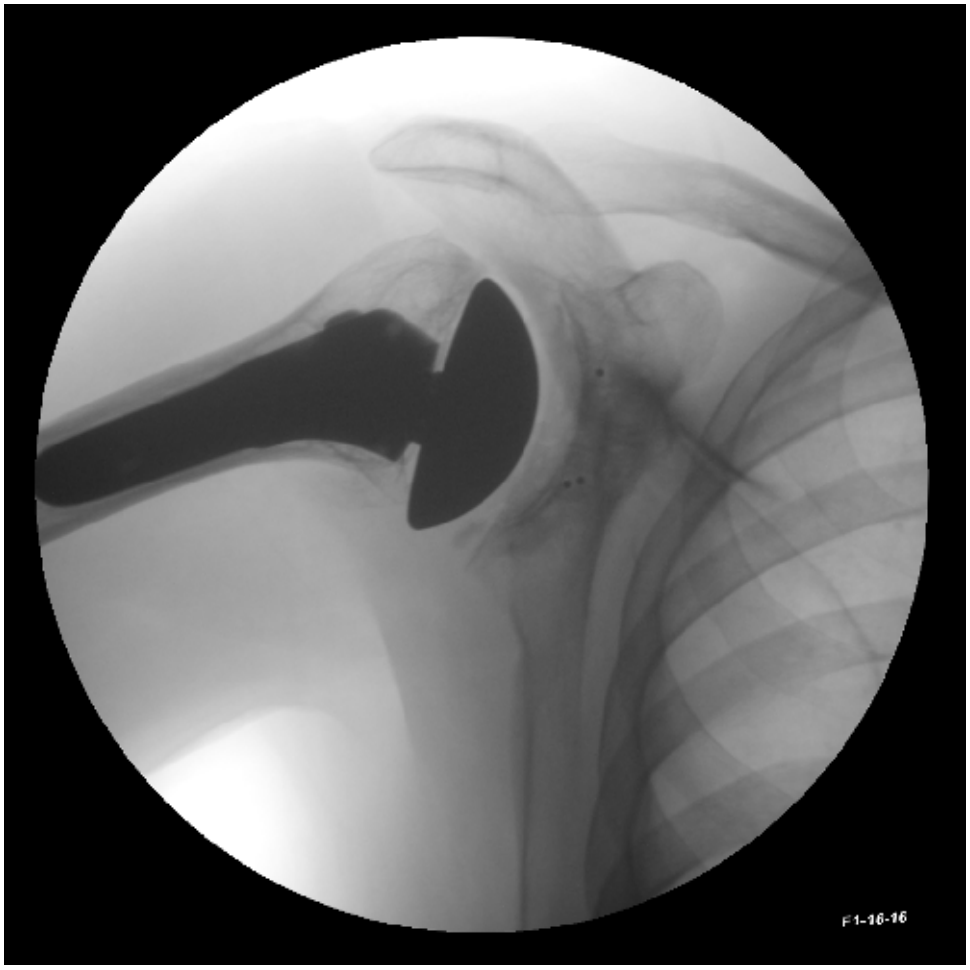

Figure 10 Typical fluoroscopic image of the shoulder with TSA.

2.3 Image Correction & Segmentation

The fluoroscopic images suffer a minimal amount of distortion in the recording process caused by perturbations of the x-ray beam from the environment and from the slightly curved surface of the image intensifier. An adapted polynomial Gronenschild[42, 43] global surface mapping technique is employed to remove the "fish-eye" caused by the curved image intensifier surface and "swirl" caused by electro-magnetic environmental disturbances. The technique is employed by mapping a set of polynomial expressions between the actual geometry of a copper grid and the acquired distorted image of the copper grid (Fig 11).

Figure 11 Typical fluoroscopic image of copper distortion correction plate.

Correction of the images is accomplished by using spatial mapping to distort the image pixels to their "correct" location based on the mapped polynomial expressions by linearly interpolating the image's intensity values (Fig 12). All image pairs acquired by the DFIS are corrected in this manner before further imaging processing.

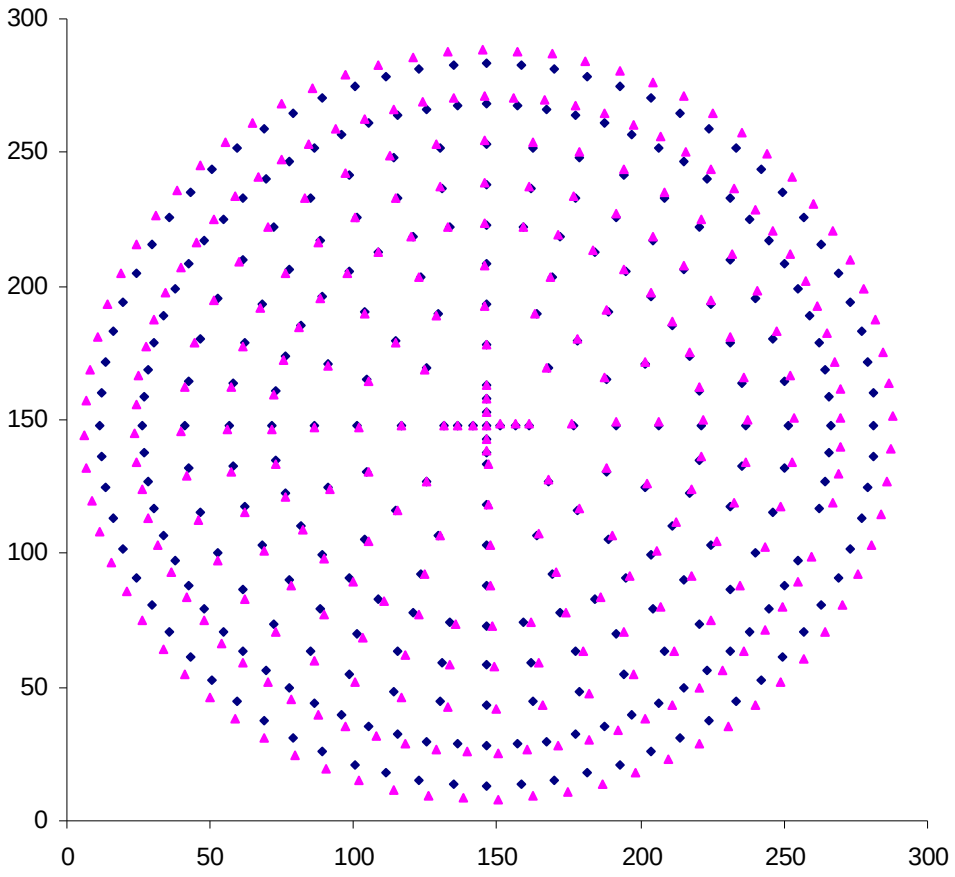

Figure 12 The actual holes in the copper plate are shown as blue diamonds. The distorted holes as imaged by the fluoroscope are shown as pink triangles. The pink triangles will be mapped to the blue diamonds using a polynomial expression. (Units in millimeters)

Next, each pair of corrected fluoroscopic images representing a unique shoulder joint kinematic pose is opened using a custom Matlab (Matlab 7.0.1, The Math Works Inc., Natick, MA) script for automated segmentation. The segmentation script is based on a Canny[44] algorithm that uses the gradient of the image's pixels intensity to

determine the outlines of objects in the image. The script has a graphical user interface so that the operator can visually check the machine's performance in correctly outlining the objects in the image (Fig 13). In some situations, human interaction is required to manually modify the machine's automated segmentation in areas where the gradient changes slower than the set threshold value. In the case of total shoulder arthroplasty, the outlines of the glenoid fixation peg beads, humeal head and stem are saved as points in a text file. The operator discards all other outlines that were automatically segmented and deemed ancillary.

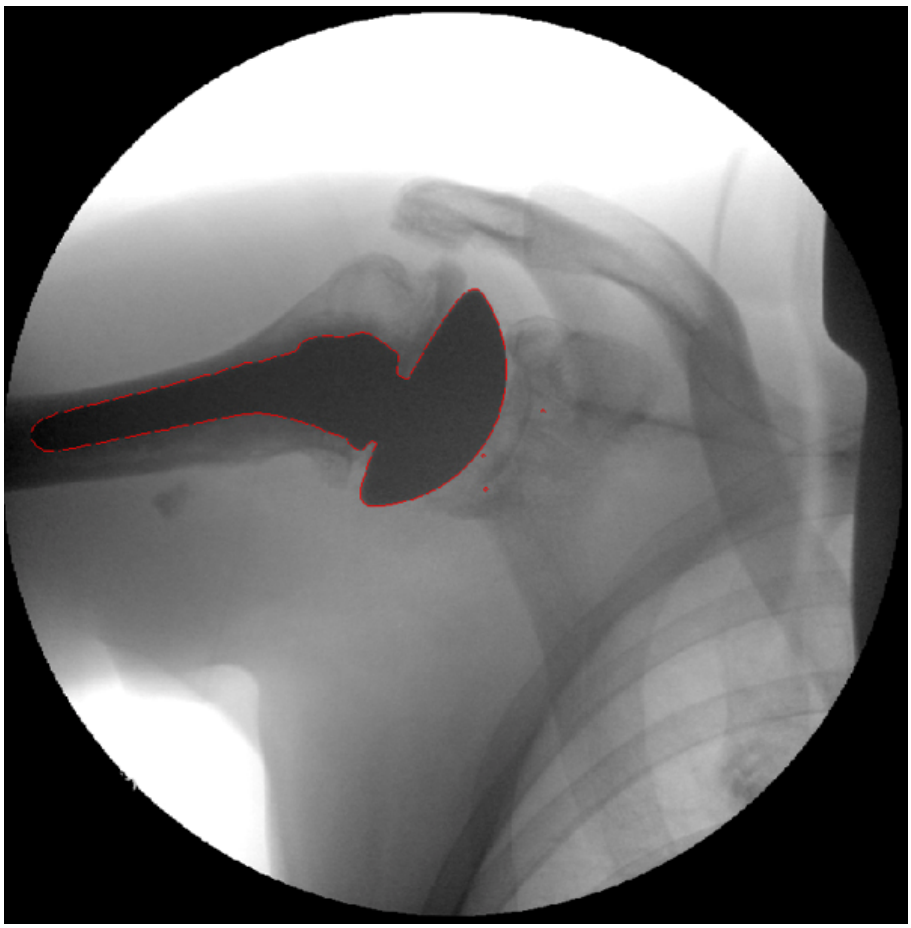

Figure 13 Typical fluoroscopic image of the shoulder with TSA after being automatically segmented and manually adjusted for ancillary outlines.

2.4 Virtual DFIS Environment & Matching

After fluoroscopic imaging of the subject's shoulder joint, calibration fixtures and image distortion correction processing, a replica of the DFIS is created in a virtual environment. This is accomplished with that data acquired from calibration images that include the location of the center of the image intensifier and the relative position of the fluoroscopes. The relative position of the fluoroscopes is determined by aligning the individual calibration solution of each fluoroscope to one another. Within solid modeling software (Rhinoceros, Robert McNeel and Associates, Seattle, WA) the aligned solution is replicated by creating two pairs of virtual sources and intensifiers such that the replicated geometry is identical to the real fluoroscopic imaging system (Fig 14).

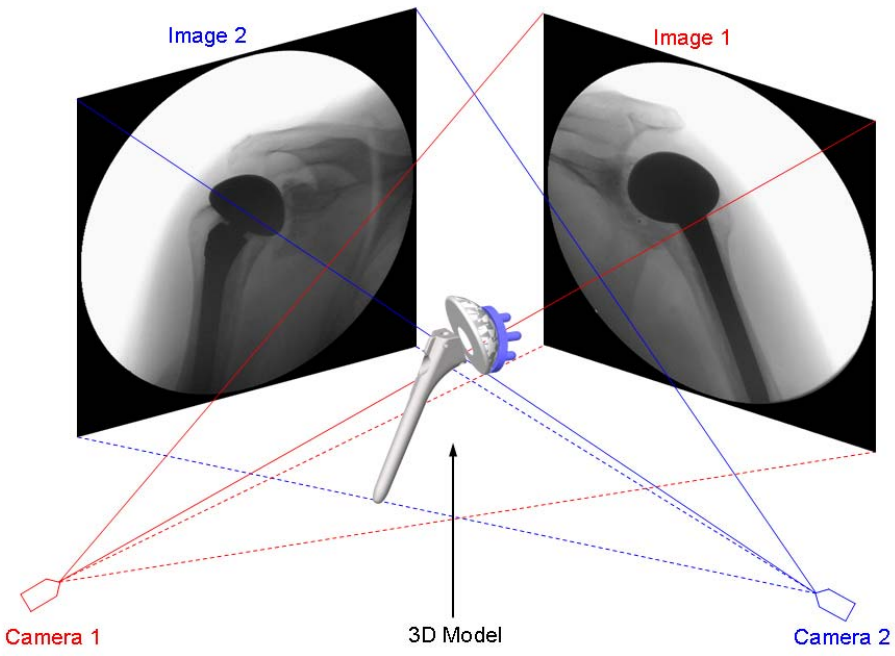

Figure 14 Virtual DFIS recreated in computer space from the geometry of the actual fluoroscopic system, shown with CAD models of total shoulder arthroplasty.

Next, the pairs of corrected fluoroscopic images and segmented outlines are imported into the virtual environment and placed on their respective virtual imaging plane. CAD models acquired from the manufacture that include the glenoid, humeral head and stem components are introduced into the virtual DFIS. A coordinate system is placed at the center of the articular surface of the glenoid component and the center of humeral head component (Fig 15).

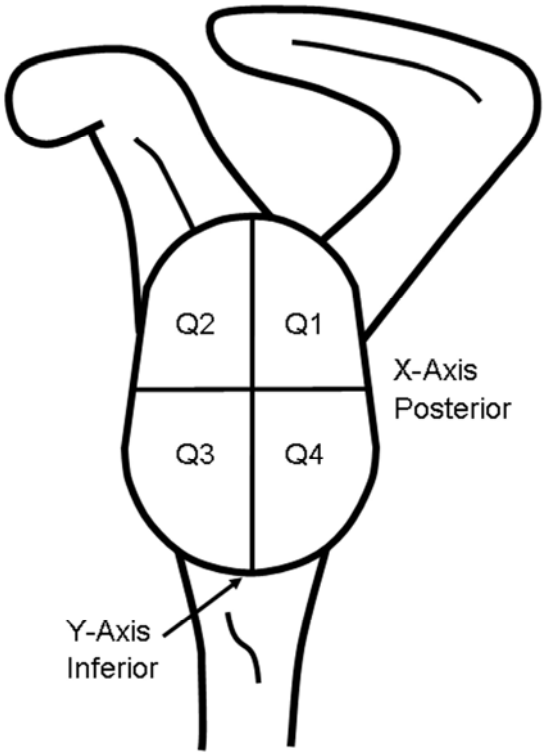

Figure 15 Left scapula shown with glenoid component. Cartesian coordinate system is created with the origin at the geometric center of the component.

All coordinate systems were defined for the left shoulder joint complex, thus to simplify data presentation, all right shoulder joints were mirrored to left shoulder joints. This procedure of importing corrected fluoroscopic images and CAD models is repeated for each selected pose that was acquired with the real DFIS. In order to recreate the in-vivo kinematics captured by the DFIS, the imported CAD models must

first be matched to the outlines on the virtual fluoroscopic image planes. This is accomplished by manually co-registering the projected silhouettes of the 3D CAD models with the 2D outlines of the fluoroscopic images. The virtual model is translated and rotated in the virtual DFIS until the 3D model matches the 2D planer images, at which point the virtual pose recreates the in-vivo pose of the subject during fluoroscopic imaging. This matching procedure is repeated for both the humeral head and stem components. The in-vivo position of the polyethylene glenoid component is recreated by orienting three radio-opaque beads inserted in the fixation pegs to their corresponding bead outlines on the fluoroscopic images. This matching technique is needed because polyethylene when imaged by a fluoroscopic imaging device in the presence of high-density radio-opaque material, such as the cobalt chromium humeral head, tends to ‘wash out’ much of the detail in the image of the glenoid. Once all poses have been recreated in the virtual environment, analysis of the coordinates systems placed on the components can be analyzed for relative motion and contact.

2.5 Accuracy & Repeatability

Previously, the accuracy of the DFIS from initial fluoroscopic imaging to measuring kinematics in the virtual environment was reported using standard geometries of a sphere and cylinder. The reported accuracies[45] were 0.1mm in translation and 0.1° in rotation. Similar accuracy is expected in the case of total shoulder arthroplasty components, where both the humeral head and glenoid fixation peg radio-opaque marker beads are spherical in geometry. However, since this research focuses on the contact location between the humeral head and glenoid surface, the accuracy of this measure is more relevant than the absolute position and will be addressed in section 2.6. Thus, an implicit relation of the absolute position is implied from the accurate measure of the contact location. To measure the repeatability of the imaging matching technique a TSA pose was chosen and the humeral head and glenoid component were independently matched 15 times each. For each trial the components were randomly oriented in the virtual DFIS, such that each subsequent match was not affected by the position of the match prior. After all independent matches were performed; a coordinate system was placed at the center of the humeral head and glenoid component. The standard deviation of the translation and rotation vectors of the coordinate system was taken as the repeatability of the system to locate each component in space (Table 1). The repeatability of the system to match both the glenoid and humeral head components were approximately the same order of magnitude for the three orthogonal translations directions and three rotations.

Glenoid Component

	Origin			Z-Axis			Normal Vector			Direction Cosines (rad)		
	x (mm)	y (mm)	z (mm)	x (mm)	y (mm)	z (mm)	I	j	k	alpha	beta	gamma
Mean	-22.53	777.22	-4.62	-20.66	779.08	5.03	1.87	1.86	9.65	1.3827	1.3841	0.2666
Std Dev	0.024	0.026	0.028	0.035	0.040	0.030	0.022	0.027	0.005	0.0022	0.0027	0.0019

Humeral Head Component

	Origin			Z-Axis			Normal Vector			Direction Cosines (rad)		
	x (mm)	y (mm)	z (mm)	x (mm)	y (mm)	z (mm)	I	j	k	alpha	beta	gamma
Mean	-15.76	782.06	11.76	-17.40	782.29	21.62	-1.65	0.24	9.86	1.7362	1.5473	0.1671
Std Dev	0.024	0.029	0.016	0.035	0.036	0.017	0.018	0.012	0.003	0.0018	0.0012	0.0018

Table 1 The mean and standard deviations reported for fifteen independent trials of matching the glenoid and humeral head components.

The system was found to have a minimum repeatability of 0.02mm in translation and 0.07° in rotation and a maximum repeatability of 0.03mm in translation and 0.15° in rotation. The larger magnitude repeatability in the rotation compared to translation is attributed the high degree of symmetry that both components share. These results are on the same order of magnitude as reported for the DFIS system and thus, the system is capable of measuring the motion of the shoulder after TSA.

2.6 Contact & Validation

One objective of this project was to use the DFIS to investigate the contact locations between the humeral head and glenoid components. The accuracy of the system was not defined by the actual position of the components, but rather the ability to accurately determine the centroid of contact. Therefore, an implicit relationship holds whereby the ability to accurately measure the contact centroid implies that a level of accuracy of the system exists such that the positions of the components in space determine the contact centroid. To verify this relationship and determine the accuracy of measuring the in-vivo glenohumeral centroid of contact by the recreated TSA joint position in the virtual environment, a silicon rubber casting technique was used [46, 47]. First, anatomical total shoulder arthroplasty components were implanted in a bone substitute and the distal diaphysis of the humerus was potted in PMMA (Poly [methyl methacrylate] bone cement). The scapula was rigidly fixed with the normal to the glenoid surface perpendicular to the ground representing roughly a 90° rotation from the anatomical position to simplify in the load application. Above the glenoid, the PMMA potted shaft of the humerus was fixed in a cylindrical jig mounted to a six degree-of-freedom load cell (160M50S; JR3 Inc, Woodland, CA, USA) attached to the manipulator of an industrial robot (UZ150F; Kawasaki Motors MFG Corp, Lincoln, NE, USA) (Fig 16). The humerus was positioned to represent approximately 60° and 90° abduction of the long axis of the humerus in neutral rotation, taking into account the scapulothoracic rotation with humeral abduction of approximately two-to-one [28, 48-51].

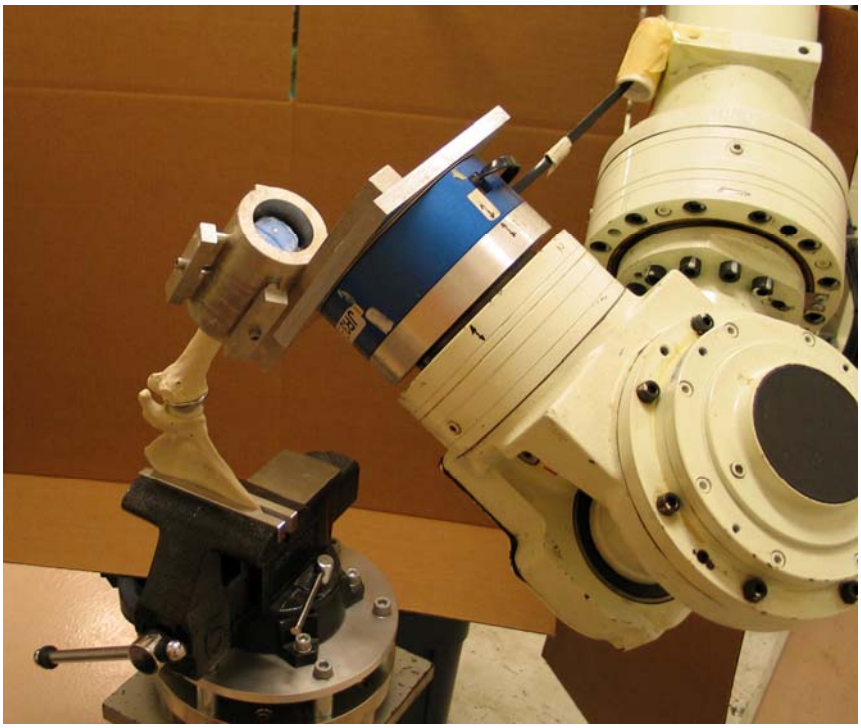

Figure 16 Contact validation setup with robotic manipulation device.

The DFIS was positioned around the glenohumeral joint. The joint was disarticulated and fast setting silicon rubber (Quick Set; Alumilite CORP; Kalamazoo, MI, USA) was placed on the glenoid articular surface, immediately followed by application of 350N from the humeral head in the direction perpendicular to the ground. A force of 350N was chosen because it was within the range of reported physiologic glenohumeral loads [24, 38, 52-56] and may approximate the holding of a ten pound weight abducted in the coronal plane. The silicon rubber set in approximately one minute. Fluoroscopic images were acquired under load and then the joint was disarticulated. The silicon rubber was squeezed out of the location where contact occurred between the humeral and glenoid articular surfaces (Fig 17). This voided area was digitized (MicroScribe® G2LX; Immersion CORP; San Jose, CA, USA) along with geometric landmarks on the glenoid component to facilitate alignment in a virtual environment

Figure 17 Silicon rubber impression.

Figure 18 MicroScribe® digitizer.

(Fig 18). Similar to the method presented earlier, a virtual DFIS was created and the fluoroscopic images corrected for distortion were imported into the virtual environment. The imaged in-vitro positions of the humerus and glenoid components were reproduced virtually and the glenoid centroids of contact measured using the overlap method described in section 3.2 of this document (Fig 19). These manual pose matching and centroid measurement protocols were repeated twelve independent times to access the repeatability of the technique. The contact centroid measured from the overlap method in the virtual environment was compared to the area centroid measured from the digitized silicon rubber casting taken as the gold standard (Fig 20). This procedure was repeated for one trial at approximately 60°

abduction and two trials at approximately 90° abduction of the long axis of the humerus in the coronal plane.

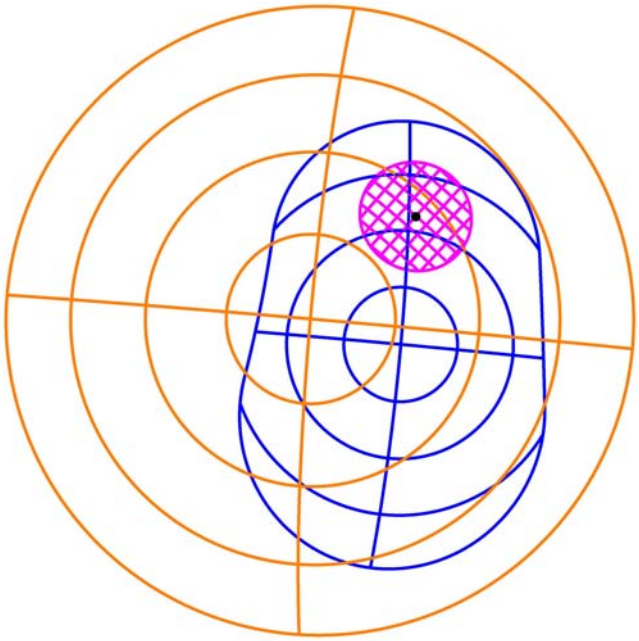

Figure 19 The overlap area of the humeral head and glenoid component is shown in pink. The black point is the centroid of the pink contact area.

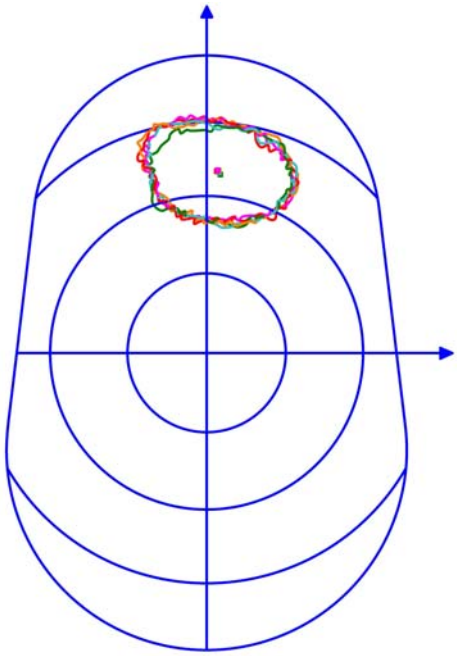

Figure 20 Digitized voided silicon area on the glenoid component.

The difference in the absolute distance of the measured centroid of contact between the overlap method and silicon rubber casting technique is listed as Delta X/Y, respectively in Table 2. To calculate delta, the average contact centroid location from the twelve independent matches was subtracted from the silicon rubber gold standard centroid location and the absolute value was taken. In general, for both X & Y directions, the average offset of the overlap method to the gold standard was at most 0.30mm, which is on the order of the accuracy of the digitizing equipment. The repeatability of measuring the contact centroid in the virtual environment was defined as the standard error of the twelve independent pose match centroid calculations and listed as SD X/Y Fluoro, respectively in Table 2. On average, for both X & Y

directions, the standard error of repeating the placement of the centroid of contact with the overlap method on the glenoid surface was approximately 0.1mm. This was on the order of the accuracy previously reported[45] for our method of reproducing in-vivo joint positions in a virtual environment. Therefore, this non-invasive fluoroscopic imaging technique can be confidently applied to determine the in-vivo glenohumeral articular contact locations in patients after TSA.

Trial	Delta X	Delta Y	SD X Fluoro	SD Y Fluoro
90° Abduction (1)	0.63	0.02	0.04	0.08
90° Abduction (2)	0.12	0.03	0.05	0.10
60° Abduction	0.15	0.22	0.05	0.18
Average	0.30	0.09	0.05	0.12
	All units in millimeters			

Table 2 Delta X and Delta Y, respectively are the difference between the calculated centroid of contact and the measured centroid using the silicon rubber technique. SD Fluoro X and SD Fluoro Y, respectively are the repeatability of locating the centroid when independently matching the glenoid and humeral components within the virtual fluoroscopic imaging system.

Chapter 3

3.1 In-Vivo Shoulder Kinematics: Application of Technique

The dual plane fluoroscopic imaging system (DFIS) has been shown to be both accurate and repeatable in the measurement of the centroid of contact of the glenohumeral joint. The non-invasive image matching technique, thus easily lends itself to studying the kinematics of the shoulder joint in the living body. Low radiation dosage from fluoroscopic imaging is the only risk that the patient encounters during the study, which has been determined to be low on the benefit-to-risk assessment performed by the Institutional Review Board (IRB) at the Massachusetts General Hospital (MGH). A cohort of 13 patients following TSA surgery was recruited for study under IRB approval. Each patient was fluoroscopically imaged with the shoulder joint in various positions representing functional shoulder motion. A virtual DFIS was recreated for each patient and the kinematics recorded during fluoroscopic imaging recreated in the virtual environment with CAD models of the joint components. Contact centroid analysis was performed and locations recorded relative to a coordinate system placed at the center of the glenoid component. The location of the center of the humeral head was measured with respect to the center of the glenoid component to investigate the coupling of the translation of the humeral head to the contact measured on the glenoid surface. These data provide a basis which to compare other surgeons' results and compare against normal contact locations in healthy individuals. The measurements may help to improve implant designs and surgical implantation technique; and ultimately to enhance component longevity and increase patients' ROM and functionality after TSA.

3.2 Total Shoulder Arthroplasty - Study Design

A total of 13 patients who underwent anatomic TSA (Anatomical Shoulder; Zimmer, Warsaw, IN, USA) from 1999-2005 were recruited from the practice of the same orthopaedic surgeon. This study was approved by the institutional review board at our institution and informed consent was obtained from all patients before participating. There were eight men and five women with an average age of 61 years (range: 37-72 years) at the time of surgery. All patients had clinically successful outcomes and were imaged for this biomechanics study at least 12 months (average: 32 months, range: 12-88 months) after the date of implantation. At the time of study, all patients were without pain and had a complete range of shoulder motion. One man had bilateral total shoulders. In total there were nine left shoulders and five right shoulders imaged (14 total). One female patient with a right TSA was not able to be analyzed due to motion artifact captured during the image acquisition process. The remaining eight men and four women with nine left and four right TSA (13 total) were investigated in this study.

Shoulder contact kinematics were measured using a dual plane fluoroscopic imaging system (DFIS) as described in section 2.2. The fluoroscopes (BV Pulsera; Philips, Bothell, WA, USA) were positioned around the shoulder of interest and allowed the patient to sit comfortably on a stool while providing ample clearance to freely move their arm without bumping the imaging system (Fig 8). A gonimeter was used to control the abduction angle (in the coronal plane) of the humerus with

respect to the sagittal plane of the body. The patient was protected from radiation exposure by custom lead aprons from the thyroid to just above the knee joint. Mirror image right and left lead vests were manufactured with lead deletes around the respective shoulder complex that allowed unobstructed fluoroscopic imaging of the joint while providing radiation protection to nearby vital organs. Each patient underwent no more than eight pairs (16 total fluoroscopic images) of simultaneous fluoroscopic images, each patient receiving a maximum of 6 mrem of ionizing radiation.

The shoulder of interest was first imaged at 0° abduction of the humerus in neutral rotation (humerus perpendicular to the ground, elbow in full extension, palm parallel to the sagittal plane) in the coronal plane while the patient sat relaxed on a stool. The patient then lifted their arm to 45° of abduction of the humerus in neutral rotation (no axial rotation of the forearm with respect to the longitudinal axis of the humerus, elbow in full extension) and was simultaneously imaged by both fluoroscopes. Similarly, the shoulder was imaged with the humerus in 90° abduction neutral rotation (elbow in full extension, palm parallel to the ground). Next the shoulder was imaged, with the humerus in 90° abduction; the patient flexed the elbow to 90° of flexion (palm parallel to the ground) and then actively rotated the shoulder into maximum external rotation. This position was similar the cocked phase of throwing motion and is the position that the shoulder is at risk for anterior instability. Finally, the shoulder was actively rotated about the longitudinal axis of the humerus in 90° abduction (elbow in 90° flexion) to maximum internal rotation, to

represent the opposite position to the cocked phase of throwing motion and simultaneous fluoroscopic images were acquired. These positions were chosen because they simulate the shoulder motion required for functional living activities such as combing one's hair. All trials were conducted under the weight of the patient's own forearm. No additional weight was held by the subject.

Using the DFIS technique described in this thesis, the geometry of the dual plane fluoroscopic imaging system was recreated in solid modeling software (Rhinoceros 4.0; McNeel, Seattle, WA, USA) to create a virtual dual plane fluoroscopic imaging system. All acquired image pairs were corrected for geometric distortion. Each patient's images were placed on their respective virtual fluoroscopic intensifier and three-dimensional CAD models of the patient's humeral head and glenoid components were introduced into the virtual environment. The position of the humeral head was manually manipulated in the virtual environment until its projections matched the outlines on the fluoroscopic images in both planes. The in-vivo position of the polyethylene glenoid component was reproduced in the virtual environment by aligning the projections from the acquired images of the radio-opaque beads implanted by the manufacturer as part of standard production in the three outermost pegs to the beads that are part of the CAD glenoid model. This procedure of recreating the in-vivo glenohumeral joint positions with CAD models in a virtual environment was repeated for all patients' image pairs acquired. The accuracy of this method to determine the six degree-of-freedom in-vivo joint positions in a virtual environment has been reported in our previous work[45], where the method

was shown to have a translational accuracy of 0.1mm and rotational accuracy 0.1° in three-dimensions.

For each recreated in-vivo glenohumeral joint position in the virtual environment, the relative motion of the humeral head to the center of the glenoid component and the centroid of articular surface contact between the CAD models of the humeral head and glenoid were determined. To determine the centroid of contact, the overlap area of the articular surfaces of the humeral head and glenoid was defined on the glenoid component articular surface and the geometric area centroid calculated. In the event that overlap between the articular surfaces was not detected, the point of minimum normal distance from the glenoid articular surface to the humeral head was defined as the contact location. This method was verified with a silicon rubber casting technique[46, 47]; details are presented in section 2.6. To quantify the humeral head motion and the contact location on the glenoid surface, a Cartesian coordinate system was placed at the geometric center of the glenoid articular surface and the humeral head component. For the glenoid, the superior-inferior axis was defined as the Y-axis and is approximately collinear with the medial scapular spine. The anterior-posterior axis was defined as the X-axis and is perpendicular to the Y-axis, shown in Figure 15. The distance ($\sqrt{X^2 + Y^2}$) from the glenohumeral contact centroid to the origin of the Cartesian coordinate system was measured for all patients in all imaged shoulder positions. To quantify the glenohumeral contact patterns of the patients, contact centroid locations were discretized into a quadrant occupancy percentage, defined as the discrete number of

contact occurrences within a quadrant to the total number of positions examined. Data presentation was made consistent by mirroring all right glenoid contact locations to left glenoid contact locations. Contact centroid locations are presented unscaled on the implanted size of the patient's glenoid component (small, medium or large).

3.3 Glenohumeral Contact Results

Patient specific TSA glenohumeral joint contacts on the glenoid component surface are shown in Figure 21. The observed contact patterns were varied among the patients as visualized by the colored coded locations. The raw data for the contact locations on the glenoid surface are shown in Table 3.

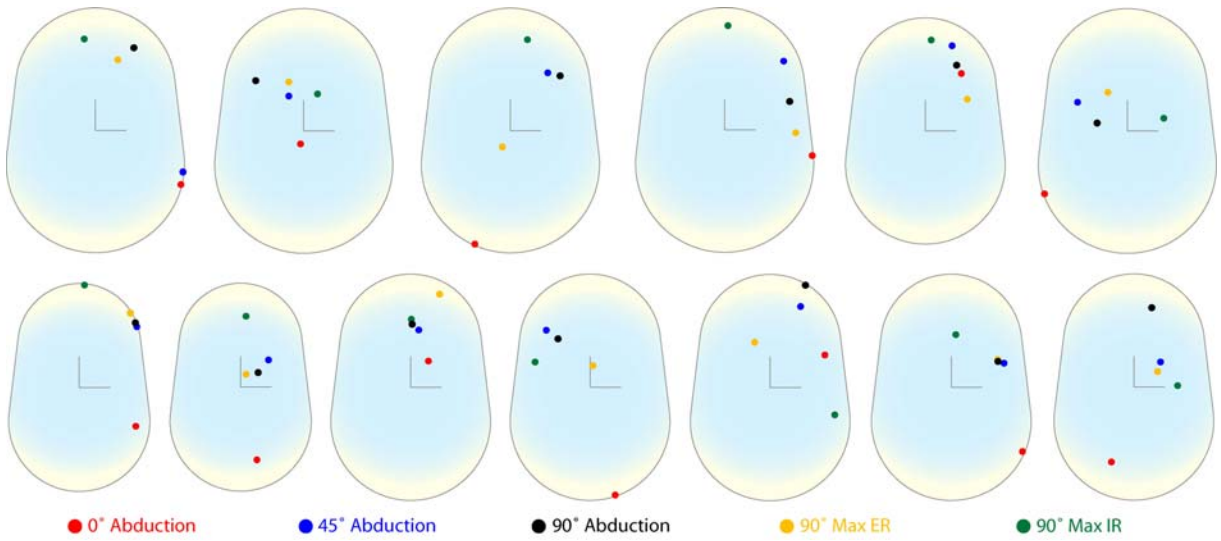

Figure 21 Unscaled patient specific contact locations on the glenoid surface as a function of arm position, shown by color code. All right shoulder contact locations were mirrored to left glenoid components.

0° to 45° abduction neutral rotation

All patients showed superior translation of the contact centroids; the average superior translation was 13.6mm. Six of 13 patients had posterior translations; the average posterior translation was 4.6mm. Seven patients showed anterior translations on the glenoid articular surface; the average anterior translation on the glenoid surface was 4.0mm.

45° to 90° abduction neutral rotation

Seven of 13 patients had superior translations; the average superior translation was 5.3mm. Six patients showed inferior translations; the average inferior translation was 2.9mm. Six of 13 patients had posterior translations; the average posterior translation was 1.6mm. Seven patients showed anterior translations on the glenoid surface; the average anterior translation was 2.7mm

90° abduction neutral rotation to maximum external rotation

Four of 13 patients showed superior translations; the average superior translation was 3.0mm. Nine patients had inferior translations on the glenoid articular surface; the average inferior translation was 5.4mm. Seven of 13 patients showed posterior translations; the average posterior translation was 3.0mm. Six patients had anterior translations; the average anterior translation was 3.9mm.

90° abduction maximum external rotation to maximum internal rotation

Eight of 13 patients had superior translations; the average superior translation was 8.4mm. Five patients showed inferior translations on the glenoid surface; the average inferior translation was 4.9mm. Five of 13 patients had posterior translations; the average posterior translation was 6.8mm. Eight patients showed anterior translations; the average anterior translation was 6.3mm.

		0°		45°		90°		Max 90ER		Max 90IR	
Patient	**Shoulder**	**X**	**Y**	**X**	**Y**	**X**	**Y**	**X**	**Y**	**X**	**Y**
1	Left	2.9	4.3	1.3	9.4	0.2	10.3	4.7	15.2	0.1	11.1
3	Left	8.9	5.3	4.9	13.2	5.7	16.7	-2.5	7.4	10.5	-4.5
4	Left	-13.5	-10.3	-8.1	4.7	-4.9	1.3	-3.2	6.3	5.9	2.1
5	Right	9.2	-6.3	9.4	9.9	9.1	10.6	8.3	12.2	0.9	16.8
6	Right	-0.5	-2.1	-2.4	5.7	-7.8	8.2	-2.4	8.0	2.3	6.1
7	Left	4.1	-17.6	-7.1	9.3	-5.2	7.9	0.5	3.5	-9.0	4.1
8	Left	2.6	-11.9	4.5	4.5	2.8	2.4	0.9	2.1	0.9	11.6
9	Right	5.9	9.4	4.3	13.9	5.1	10.7	6.8	5.2	0.9	14.9
9	Left	14.3	-4.2	9.6	11.3	10.6	4.7	11.6	-0.4	0.5	17.1
10	Left	13.9	-8.9	14.3	-6.8	6.3	13.5	3.7	11.5	-1.8	14.9
11	Left	-5.8	-18.6	6.1	9.4	8.1	8.9	-1.3	-2.7	2.8	14.8
12	Left	-3.7	-12.3	4.3	4.1	2.9	13.0	3.9	2.5	7.1	0.2
13	Right	11.6	-10.5	8.6	3.9	7.6	4.2	7.6	4.5	0.7	8.6
All units in millimeters											

Table 3 The locations of the glenohumeral contact on the glenoid surface. The data is not scaled for component size. Data presentation is made consistent by mirroring all right shoulders to left glenoid components.

In all 65 positions examined, no contact was found at the geometric center (origin) of the glenoid component (Table 4). In all positions, the centroid of articular contact was on average 11.0 ± 4.3mm away from the center of the component. Contact locations in 0° abduction of the humerus in neutral rotation were on average the furthest away from the center of the glenoid at 12.8 ± 5.0mm. The contact centroids in 90° abduction of the humerus in the coronal plane with maximum active external rotation were on average the closest to the glenoid center at 8.3 ± 4.4mm.

Shoulder	1	2	3	4	5	6	7	8	9	10	11	12	13	Average	Std Dev	Min
0°	5.2	10.4	17.0	11.2	2.2	18.1	12.2	11.1	14.9	16.5	19.4	12.8	15.6	12.8	5.0	2.2
45°	9.5	14.1	9.4	13.6	6.2	11.7	6.4	14.6	14.8	15.8	11.2	6.0	9.5	11.0	3.5	6.0
90°	10.3	17.7	5.1	14.0	11.3	9.5	3.7	11.9	11.6	14.9	12.1	13.3	8.7	11.1	3.8	3.7
Max 90ER	15.9	7.8	7.1	14.7	8.4	3.6	2.3	8.6	11.6	12.1	3.0	4.6	8.8	8.3	4.4	2.3
Max 90IR	11.1	11.4	6.3	16.8	6.5	9.9	11.6	14.9	17.1	15.0	15.1	7.1	8.6	11.6	3.9	6.3
	All units in millimeters															

Table 4 Radial distance of the contact centroid from the center of the glenoid component. Data is not scaled for glenoid component size.

Glenohumeral joint contact was predominantly on the superior-posterior quadrant (Q1) of the glenoid surface representing 61.5% of the total contact for all positions (Fig 22). 21.5% (14 of 65) of the total contact was inferior to the glenoid horizontal midline, 10 of these 14 contacts were at 0° abduction neutral rotation. Quadrant three, the inferior-anterior quadrant saw only 7.7% (5 of 65) of the total contact, where four of these five contacts were at 0° abduction neutral rotation. The other (1 of 5) contact in quadrant three was at 90° abduction with maximum active external rotation (Fig 23). In 45° abduction, only one patient had contact in the inferior-posterior (Q4) quadrant, this same patient had contact in Q4 at 0° abduction, the distance between the contact centroids was 2.08mm. In general, the contact frequency distributions were similar for all shoulder positions except 0° abduction of the humerus in the coronal plane with neutral rotation. If we ignore this position, 92.3% (48 of 52) of the glenoid contact was superior to the horizontal midline with active abduction of the humerus.

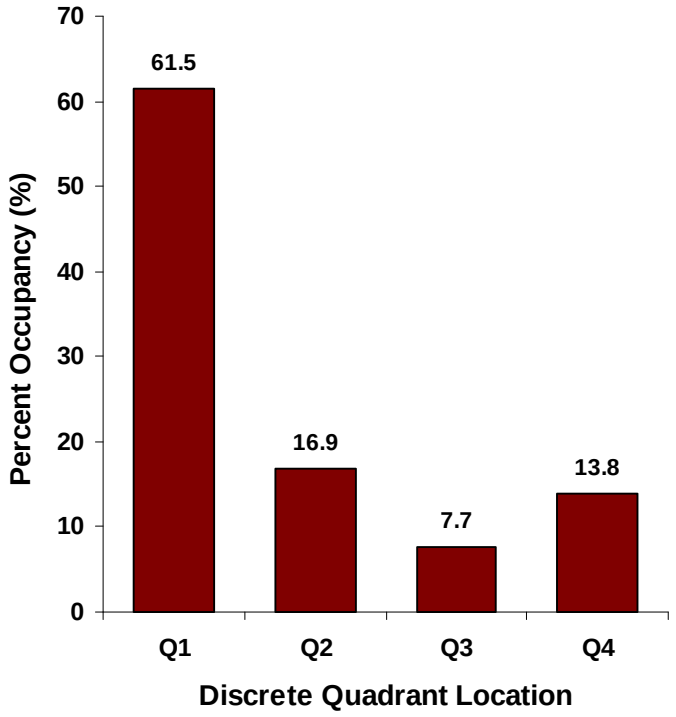

Figure 22 Percent occupancy per quadrant to all shoulder positions imaged.

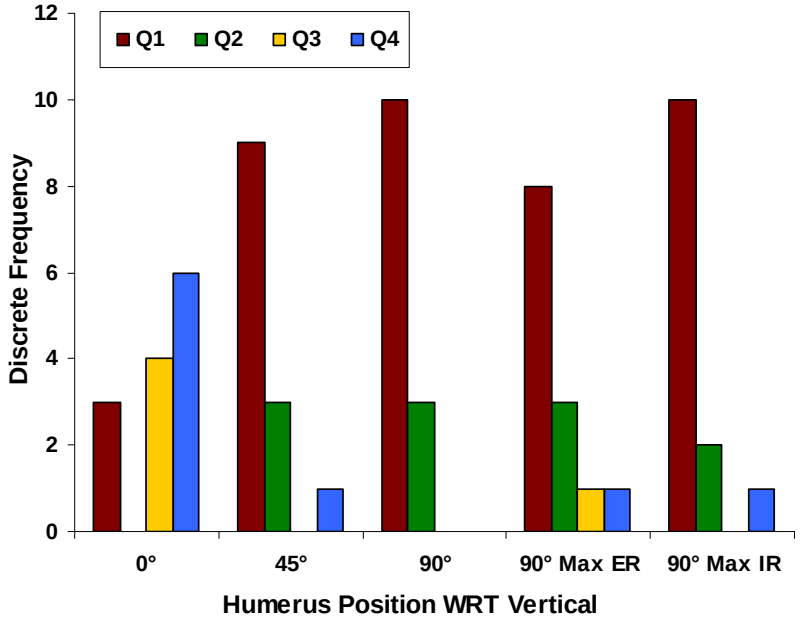

Figure 23 Discrete frequency of quadrant contact per shoulder position imaged.

3.4 Humeral Head Kinematics Results

Patient specific humeral head center locations on the glenoid component surface are shown in Figure 24. The observed humeral head center locations were varied among the patients as visualized by the colored coded locations. The raw data for the contact locations on the glenoid surface are shown in Table 5.

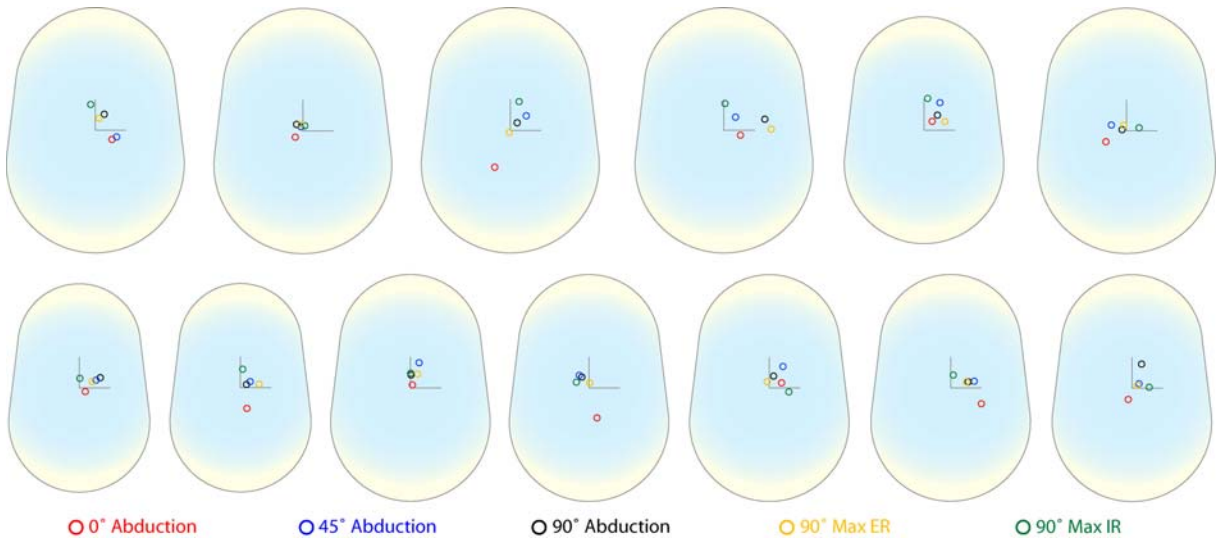

Figure 24 Unscaled patient humeral head center locations on the glenoid surface as a function of arm position, shown by color code. All right shoulder humeral head centers locations were mirrored to left glenoid components.

0° to 45° abduction neutral rotation

All patients showed superior translation of the humeral head center relative to the center of the glenoid; the average superior translation was 3.5mm. Ten of 13 patients had posterior translations; the average posterior translation was 1.4mm. Three patients showed anterior translations of the humeral head center; the average anterior translation was 1.6mm.

45° to 90° abduction neutral rotation

Four of 13 patients had superior translations of the humeral head center; the average superior translation relative to the center of the glenoid was 1.9mm. Nine patients showed inferior translations; the average inferior translation was 1.0mm. Five of 13 patients had posterior translations; the average posterior translation was 1.6mm. Eight patients showed anterior translations of the humeral head center; the average anterior translation was 1.1mm

90° abduction neutral rotation to maximum external rotation

Three of 13 patients showed superior translations; the average superior translation was 0.3mm. Nine patients had inferior translations of the humeral head center relative to the glenoid; the average inferior translation was 1.2mm. One patient did not translate superior-inferior during this shoulder position. Seven of 13 patients showed posterior translations; the average posterior translation was 1.1mm. Six patients had anterior translations; the average anterior translation was 0.9mm.

90° abduction maximum external rotation to maximum internal rotation

Nine of 13 patients had superior translations; the average superior translation was 2.2mm. Four patients showed inferior translations of the humeral head center relative to the glenoid; the average inferior translation was 0.6mm. Five of 13 patients had posterior translations; the average posterior translation was 2.0mm. Eight patients showed anterior translations; the average anterior translation relative to the center of the glenoid was 2.7mm.

		0°		45°		90°		Max 90ER		Max 90IR	
Patient	**Shoulder**	**X**	**Y**	**X**	**Y**	**X**	**Y**	**X**	**Y**	**X**	**Y**
1	Left	0.3	0.5	1.4	4.1	0.1	2.1	1.2	2.3	0.0	2.4
3	Left	2.0	0.9	2.2	3.5	0.7	2.0	-0.3	1.0	3.2	-0.6
4	Left	-3.4	-1.8	-2.5	0.9	-0.7	0.2	-0.5	0.9	2.0	0.5
5	Right	1.0	-0.6	2.7	1.3	3.4	1.7	2.1	1.0	0.1	1.6
6	Right	-1.3	-1.0	-0.3	0.7	-1.0	1.1	-0.3	1.1	0.3	0.9
7	Left	1.3	-4.9	-1.6	2.1	-1.2	1.8	0.1	0.8	-2.1	0.9
8	Left	1.1	-3.4	1.6	1.0	1.0	0.5	3.0	0.6	0.4	3.0
9	Right	1.3	1.4	2.6	4.5	2.2	2.5	3.4	1.4	0.6	5.2
9	Left	2.7	-0.8	1.9	2.2	6.7	1.8	7.7	0.2	0.2	4.4
10	Left	2.7	-1.5	3.5	-1.1	1.5	2.6	0.6	1.9	-0.7	4.2
11	Left	-2.5	-6.0	2.6	2.4	1.1	1.2	-0.2	-0.3	1.4	4.7
12	Left	-0.6	-1.8	1.2	0.7	1.6	3.9	0.9	0.4	2.8	0.1
13	Right	5.0	-2.6	3.8	1.1	2.8	1.0	2.6	1.0	0.4	2.1
All units in millimeters											

Table 5 The locations of the humeral head center on the glenoid surface. The data is not scaled for component size. Data presentation is made consistent by mirroring all right shoulders to left glenoid components.

In all 65 positions examined, the humeral head center was not centered at the geometric center (origin) of the glenoid component (Table 6). In all positions, the center of the humeral head was on average 2.8 ± 1.6mm away from the center of the glenoid component. Humeral head centers in 0° abduction of the humerus in neutral rotation were on average the furthest away from the center of the glenoid at 3.1 ± 1.8mm. The contact centroids in 90° abduction of the humerus in the coronal plane with maximum active external rotation were on average the closest to the glenoid center at 2.3 ± 1.9mm.

Shoulder	1	2	3	4	5	6	7	8	9	10	11	12	13	Average	Std Dev	Min
0°	0.6	2.2	3.8	1.2	1.6	5.0	3.5	2.0	2.8	3.1	6.5	1.9	5.6	3.1	1.8	0.6
45°	4.3	4.2	2.7	3.0	0.8	2.6	1.9	5.2	2.9	3.6	3.5	1.4	4.0	3.1	1.3	0.8
90°	2.1	2.1	0.8	3.8	1.5	2.1	1.1	3.3	6.9	3.0	1.7	4.2	3.0	2.7	1.6	0.8
Max 90ER	2.6	1.1	1.0	2.4	1.1	0.8	3.1	3.7	7.7	2.0	0.4	1.0	2.8	2.3	1.9	0.4
Max 90IR	2.4	3.2	2.1	1.6	0.9	2.3	3.0	5.2	4.4	4.3	4.9	2.8	2.1	3.0	1.3	0.9
	All units in millimeters															

Table 6 Radial distance of the center of the humeral head from the center of the glenoid component. Data is not scaled for glenoid component size.

The humeral head center was predominantly on the superior-posterior quadrant (Q1) of the glenoid surface representing 63.1% of the total contact for all positions. 20.0% (13 of 65) of the total contact was inferior to the glenoid horizontal midline, 10 of these 14 contacts were at 0° abduction neutral rotation. Quadrant three, the inferior-anterior quadrant saw only 7.7% (5 of 65) of the total contact, where four of these five contacts were at 0° abduction neutral rotation. The other (1 of 5) contact in quadrant three was at 90° abduction with maximum active external rotation. In general, the contact frequency distributions were similar for all shoulder positions except 0° abduction of the humerus in the coronal plane with neutral rotation. If we ignore this position, 94.2% (49 of 52) of the glenoid contact was superior to the horizontal midline with active abduction of the humerus.

3.5 Coupled Motion

Patient specific glenohumeral contact locations on the glenoid and humeral head center locations on the glenoid component surface are shown in Figure 25. The glenoid contact locations translated on the glenoid surface in the same direction as the humeral head center, but at a smaller magnitude as visualized by the colored coded locations. The raw data for the contact locations and humeral head centers on the glenoid surface are shown in Table 3 and Table 5, respectively.

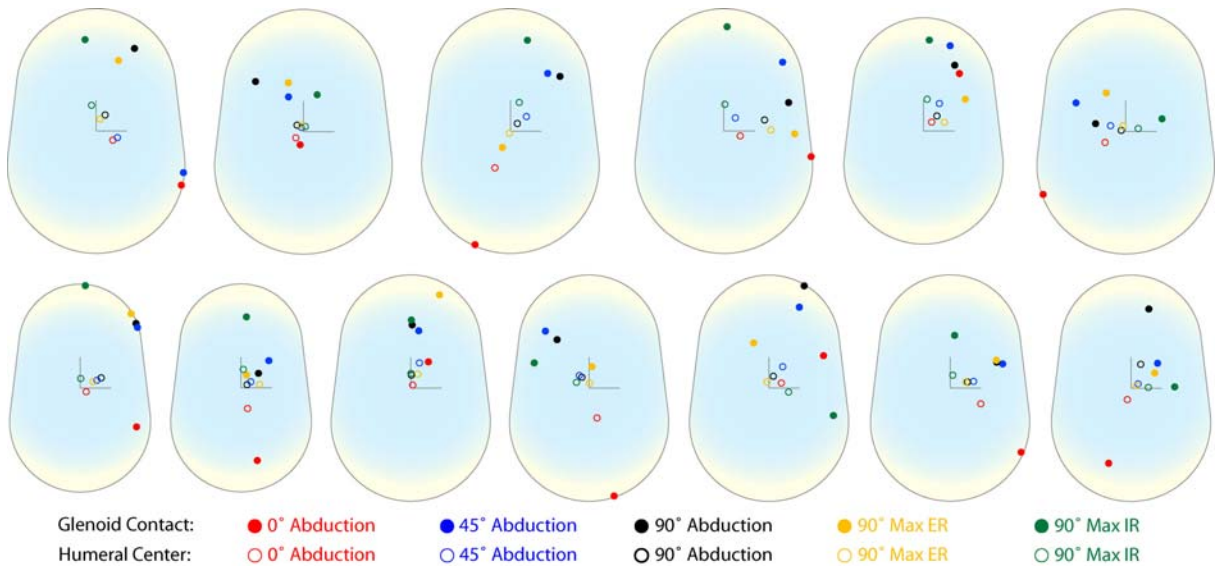

Figure 25 Unscaled patient specific glenoid contact locations and humeral head center locations on the glenoid articular surface as a function of arm position, shown by color code. All right shoulder locations were mirrored to left glenoid components.

The direction of the glenohumeral contact centroid followed the direction of the humeral head center (Fig 25). The glenohumeral contact translation in the X direction was on average 2.6 times greater than the translation of the humeral head center. Similarly, the glenohumeral contact translation in the Y direction was on

average of 4.0 times greater than the translation of the humeral head center (Fig 26). Both X and Y slope linear regressions were found significant at p<0.001.

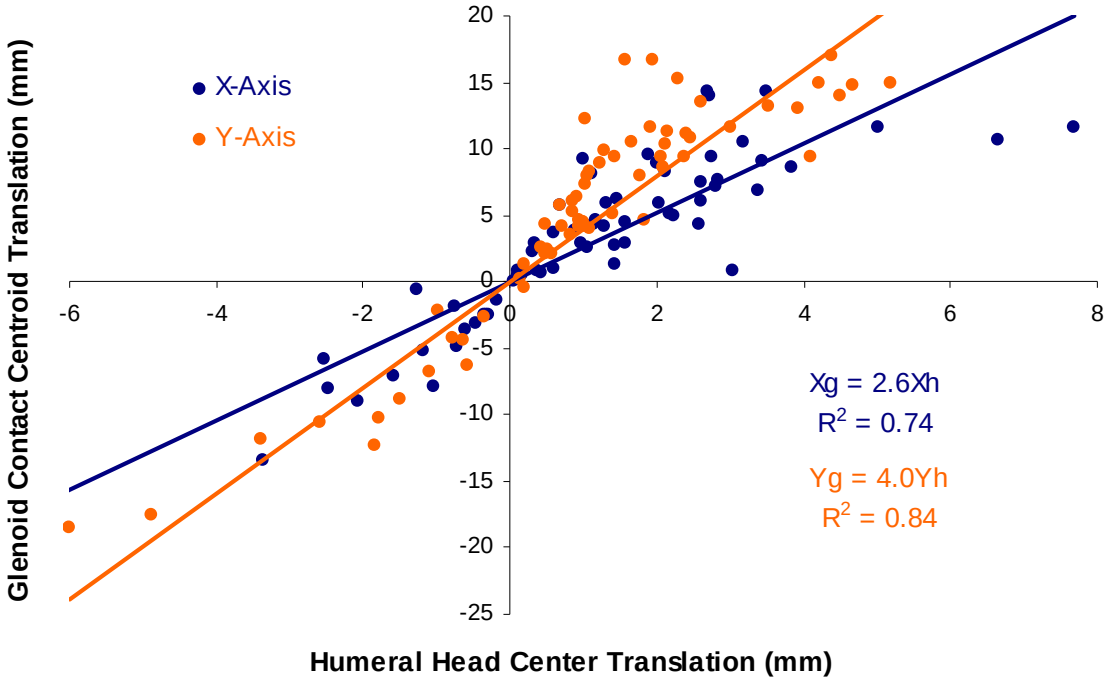

Figure 26 Plot of the glenoid contact centroid translation versus the humeral head center translation, showing the ratio of glenohumeral contact translation to the humeral head in X and Y directions.

The ratio of the X coupling to the Y coupling of the glenoid contact location to the center of the humeral head is given by: $\frac{2.6}{4.0} = 0.65$

The ratio of the average physical dimensions of the glenoid cavity is[10]:

$$\frac{23mm + 29mm}{2\,(39mm)} = 0.67$$

The amount of measured translation in patients after TSA of the glenoid contact location to the humeral head center is approximately proportional to the physical dimensions of the glenoid component as shown by comparing the ratios 0.65 ~ 0.67.

3.6 Discussion - Comparison With Previous Results

A restored range of motion, pain relief[1] and durability are primary outcomes sought by patients after TSA for treatment of end-stage shoulder degeneration. The prosthetic shoulder implant design and surgical technique together help facilitate these patient goals. However, component failures, such as glenoid loosening and polyethylene damage have been reported in the literature[3-7]. To this end, in-vivo glenohumeral joint contact kinematics are necessary for the improvement of implant design and surgical implantation technique; and ultimately to enhance component longevity. Therefore, the purpose of this study was to quantify the glenohumeral kinematics in patients after anatomic TSA and report their humeral head center translations and glenoid contact locations using a non-invasive dual plane fluoroscopic imaging technique. In doing so, we proved our null hypothesis that anatomic TSA glenohumeral articular joint contact is not centered on the glenoid surface. Furthermore, there was contact variation among the patients and contact centroids translated significantly on the glenoid surface demonstrating that contact kinematics are not 'ball-in-socket' as traditionally thought[17, 24, 26-28].

Several cadaveric studies have documented the healthy glenohumeral articular contact locations in-vitro, however no study has reported on TSA contact kinematics. For example, Conzen and Eckstein[57] in cadavera without shoulder pathology used FUJI Prescale film to show that only parts of the glenoid fossa exhibit contact under load, they reported both central and bicentric (superior-inferior) contact

areas. Specifically, during normal abduction in the scapular plane without external rotation, they found 3 of 10 glenohumeral joints with central contact, 4 of 10 with bicentric (superior-inferior) contact and 3 of 10 with mixed contact areas. They reported that with increasing abduction of the humerus there was a superior migration of the contact area in the specimens with central contact patterns (3 of 10). Additionally, they reported that superior migration was found in the joints of bicentric (superior-inferior) load-bearing areas (4 of 10), but that this was less obvious than with the central contact area specimens. Likewise, Soslowsky et al. found with a sterophotogrammetry analysis[58] that at 0° abduction in the humeral starting rotation, contact on the glenoid was split 74% anterior and 26% posterior. They found that as the humerus increased abduction, the contact area shifted slightly posterior. Thus, at 60° abduction, the contact was 63% anterior and 37% posterior, and at 120° abduction, the contact was 62% anterior and 38% posterior, and finally at 180° abduction, the contact was 37% anterior and 63% posterior. Additionally, Soslowsky et al. described a slight inferior shift of contact on the glenoid fossa with increasing abduction of the humerus from 0° to 180° abduction.

The results of Conzen and Eckstein[57] are contrasted with our present study where we report that the majority of contact is in the superior-posterior quadrant of the glenoid component, as opposed to central or superior-inferior contact. Also, we did not observe any bicentric or multi-point contact on the glenoid surface, which may be explained by the rigid materials of shoulder prosthetics compared to natural compliant articular cartilage. Soslowsky et al. report[58] that at 0° abduction,

approximately 38% of the contact was on the inferior glenoid surface, however we found 77% (10 of 13) of contact on the inferior glenoid surface. Additionally at 0° abduction, Soslowsky et al. report approximately 51% of the contact in the superior-anterior quadrant of the glenoid surface; in contrast we found no contact in this shoulder position and quadrant.

However, the results presented in this thesis do parallel a previous study conducted in our lab[59] where we reported that the in-vivo glenohumeral joint contact centroids of healthy volunteers are not centered and translated significantly on the glenoid surface. We also found similar contact frequencies for the inferior-anterior quadrant, having reported a 4% (1 of 25) contact frequency in the normal subjects and a 7.7% (5 of 65) contact frequency in anatomic TSA patients. These results suggest that anatomic TSA shoulder mechanics do not follow 'ball-in-socket' motion and result from the recreated anatomic glenohumeral geometry. The recreated glenohumeral anatomy in TSA patients is accomplished through the correct sizing of the humeral and glenoid components coupled with surgical implantation in an anatomic orientation. Anatomically designed shoulder components incorporate a radial mismatch[4, 5, 13, 25, 60] between the radius of curvature of the humeral head and glenoid articular surface to mimic the radial mismatch between the articular cartilage surfaces of the native joint[10-12, 17]. This radial mismatch in anatomic TSA allows the implanted humeral head component to translate on the glenoid surface just as found in the healthy volunteer shoulders, thereby recreating a normal motion pattern that is not 'ball-in-socket.'

The observed contact patterns in this study, specifically the preferred contact in the superior-posterior quadrant of the glenoid surface representing 40 of 65 total positions imaged is not explained from the anatomic geometry alone. Because the geometric symmetry of the components should not favor any one quadrant on the glenoid surface, when the concave, convex and compressive nature of the glenohumeral joint should favor centered contact, which our study has shown otherwise. In support of this preferred contact, retrieval studies have found significant damage in the superior-posterior portion of retrieved glenoid components[6, 7]. The reason for preferred superior-posterior contact in TSA patients is currently unknown; although several factors could be soft tissue balance of the rotator cuff, glenoid version and prioprecceptive neuromuscular control. Nevertheless, 0° abduction of the humerus with neutral rotation in the coronal plane exhibited the greatest variation of contact quadrant frequency, yet no contact was found on the superior-anterior quadrant. In general, the contact centroids at 0° abduction were the most inferior of all positions imaged and may result from a lack of isometric muscle contraction (relaxed muscles) needed to maintain this arm position compared to the other arm positions studied, thus allowing the humeral head to translate inferiorly on the glenoid surface. To delineate this inferior contact phenomenon, future studies should ask the patient to shrug their shoulder in this position, both with and without additional weight held in the hand.

Previous studies have investigated the motion of the center of the humeral head relative to the glenoid center. Poppen and Walker[28] used plane film two

dimensional x-rays to investigate the in-vivo superior-inferior motion, reporting that the average translation was 1.09 ± 0.47mm. Harryman et al. investigated the three dimensional translation of the humeral head center using a magnetic tracking system in cadavers[23]. Using an MRI technique Rhoad et al. reported the in-vivo motion in the anterior-posterior direction as ±2.1mm and the superior-inferior direction ±1.7mm away from the center of the glenoid[61]. Similarly Schiffern et al. using an MRI testing protocol measured the in-vivo anterior-posterior translation as 1.9mm in the anterior direction and 2.2mm in the posterior direction[62]. The various reported values for the translation of the humeral head center can possibly be attributed to the measuring techniques. For MRI measurements, the patient is lying supine and the shoulder is held in the position of interest for several minutes for each pose image. By having the patient lie supine, the direction of gravity is changed from acting in the superior-inferior direction to the anterior-posterior and may affect the amount of measured translation. In addition, the shoulder is supported in the MR machine for each pose and may allow the muscles of the rotator cuff to relax causing the measured translations to be greater than they would be under dynamic conditions.

Comparing the measured humeral head translations after TSA found in this study to that of previous studies is challenging because the motions of the shoulder were different for each study. However, for all positions examined (65 total) the average anterior-posterior location and average translation was 1.2mm ± 2.0mm and the average superior-inferior location and average translation was 1.0mm ± 2.1mm. Thus on average the location of the center of the humeral head was 1.2mm posterior

and 1.0mm superior, which is consistent with having 63.1% of the humeral head center locations in the superior-posterior quadrant. The average translations are similar to those previously reported[61, 62] and may suggest that the amount of humeral head translations are relatively insensitive to measurement technique and shoulder position. The data suggests the center of the humeral head remains relatively centered on the origin of the glenoid component within approximately ±2mm in both the X and Y direction. However, this small translation is not 'ball-in-socket' which implies that the contact centroid of the glenoid and humeral head remain centered on the glenoid component. This coupling of the translation of the humeral head and the glenoid contact location was shown in Figure 25, where the location of the humeral head center directly effected the location of the contact. Such that, the observed strong translational coupling between the humeral head center and glenohumeral articular contact centroid shows that for small translations of the humeral head center the glenoid contact can shift significantly on the glenoid articular surface; thus indicating the effect of glenohumeral radial mismatch[4, 5, 13, 25, 60] on shoulder joint contact biomechanics.

The effect of radial mismatch was investigated, although the low sample size of 13 shoulders was not significant to find how the radial mismatch may influence the translation of the humeral head on the glenoid surface after TSA. Walsh et al. has said that the ideal radial mismatch is between 5mm and 7.5mm, although these values were determined primarily from minimizing the radiolucency of the glenoid component in the scapula bone and not from understanding the translations of the

humeral head and the effect on the glenohumeral contact location[4, 63]. A radial mismatch of 2.7mm to 7.4mm was recorded for the 13 patients investigated in this study. There was not a relationship between the radial mismatch and the observed translation of the humeral head. Future studies should include a large sample of patients with a wide range of radial mismatches to discern how the mismatch amount may affect the magnitude of the humeral head center and the amount of influence that the translation of the humeral head has on the contact centroid of the glenohumeral joint. These results may have significant implications for component designs and the ultimate longevity of the components.

Chapter 4

4.1 Discourse

This work quantified for the first time the in-vivo glenohumeral joint contact locations and humeral head centers in patients after TSA using a non-invasive three-dimensional image matching technique. The glenohumeral contact locations and humeral head translations are unique to the 3D ability of the technique presented in this thesis. Previous studies have sought to quantify the humeral head translations relative to the glenoid in both normal and TSA patients, however, the limitations of the previous methods[23, 28, 61, 62] may reduce the clinical and biomechanical impact of the results. The previous methods can be broken down to in-vitro and in-vivo assessments. In-vitro measurements have the advantage of using invasive measurement techniques, but suffer from the lack of dynamic physiological muscle loading. The absence of muscle loading significantly alters the humeral head translations and thus effects the glenohumeral contact locations. Current in-vivo techniques for measuring humeral head translations, however sophisticated, suffer from limited accuracy and 3D analysis. Thus the techniques presented in this work address the short comings of previous in-vitro and in-vivo analysis of shoulder joint kinematics. The method presented provides a structured approach for measuring the in-vivo shoulder kinematics under physiological loading conditions to analyze humeral head translations and glenohumeral joint contact locations.

4.2 Advantages & Limitations

Although this thesis seeks to address the limitations of previous research, the study design is not without its own set of limitations. Our patient population was limited to 13 clinically successful TSA operations and their resultant contact kinematics without distinguishing gender and dominance differences. The relative implanted position of the glenoid component to the glenoid vault orientation with respect to preoperative x-ray or CT image studies and its effect on glenohumeral contact locations was not assessed. Thus, the amount of glenoid version and superior-inferior tilt corrected for in the reaming process of the TSA procedure could not be correlated to posterior contact on the glenoid articular surface. In addition, all shoulder orientations examined in this study were imaged under static conditions by the dual plane fluoroscopic imaging system. However, the patient was required to dynamically stabilize and position their arm to the desired shoulder orientation of interest and actively hold this pose for approximately five seconds for image alignment and acquisition. Glenohumeral joint loading was under forearm weight only; no additional weight was held by the patients during abduction and internal and external rotation motions. Future studies should quantify gender and dominance differences, the effect of glenoid version on contact centroids, dynamic glenohumeral joint contact motion and the effect that increased glenohumeral loading has on contact locations.

Another limitation of this study revolves around the overlap method for determining the contact centroid between the glenoid and humeral head component. Specifically the dimensional differences between the components CAD models and the machined parts tolerances that coupled with the positional accuracy of the components placement in the virtual environment affect the amount of component overlap and thus the location of the contact centroid. However, rigorous validation of this method is presented in section 2.6 and shows that in spite of these technical challenges, the overall system's ability to measure the contact centroid location is highly repeatable and accurate. This overlap method was applied to 48 of 65 positions in the virtual environment, 17 other shoulder positions did not show overlap between the glenoid and humeral head components. In these 17 cases, the minimum normal distance between the components articular surfaces were found and defined as the contact centroids. For these reasons, it is important to remember that this thesis presents the centroids of contact and not that of actual contact areas of the glenohumeral joint following TSA. Nonetheless, the data from this study may provide an insight to shoulder biomechanics and help with understanding damage mechanisms of the polyethylene glenoid component in-vivo.

4.3 Future Work

The data and validated technique from this thesis provide the insight necessary to investigate other shoulder joint related kinematics questions. The non-invasive image matching technique was modified to use cinematic fluoroscopic image acquisition in place of static image capture as recorded in the glenohumeral contact locations presented in this work. Cinematic image capture allows the real-time dynamic motion capture of the shoulder joint at 30, 15 and 8 images per second at a uniform distribution. This method was applied to investigate the dynamic scapulothoracic kinematics in a patient after TSA. The results are the first to suggest that the relative contribution of the glenohumeral and scapulothoracic joints on abduction and adduction may not be constant as previously thought. Similarly, the DFIS was validated using a cadaver model to assess the systems ability to accurately track bone models compared to the bead tracking method taken as the 'gold standard' during dynamic motion of the shoulder joint complex. The assessment has shown that the DFIS is accurately able to measure the kinematics of the native joint non-invasively and opens the door to investigate real life problems such as understanding the kinematics of throwing a baseball or lifting a weight. In addition, these data provided a validated and accurate technique that can be used to apply for grant funding and investigate larger populations to establish a database of 'normal' shoulder motion which can be used as the comparison for future studies of pathologic shoulder conditions to investigate the effect that surgical modalities and treatment efficacies have on the restoring shoulder joint motion.

4.3.1 Dynamic Scapulothoracic Kinematics After TSA

Introduction

Preserving scapular function following total shoulder arthroplasty (TSA) is essential for maintaining the normal range of dynamic motion of the shoulder joint complex. However, the ability to accurately measure in-vivo glenohumeral and scapular motion remains a challenge in the field of bioengineering. Single plane radiography was used to explore scapular rotation, but is limited to motion parallel to the imaging plane[50]. Bi-plane x-ray systems have been developed to overcome this limitation; however, these systems can suffer from relatively high radiation dosages[41, 64]. To minimize these effects, 6DOF electromagnetic tracking devices have been attached to the shoulder joint complex to measure scapulothoracic kinematics; except at large humeral abduction angles they can suffer skin motion artifacts[65, 66]. The purpose of this study was to investigate the feasibility and repeatability of using dual orthogonal cine fluoroscopy to quantify the dynamic scapular motions of living subjects after anatomic TSA.

Material and Methods

One TSA patient with anatomical shoulder components (Anatomical Shoulder System, Zimmer, Warsaw, IN) was recruited under IRB guidelines and informed consent. The replaced shoulder was scanned at 30 frames per second while the patient performed dynamic abduction and adduction in the field of view of two fluoroscopes (BV Pulsera, Philips, Bothell, WA). The shoulder was scanned in a cycle from approximately 27° to 55° abduction/adduction over a period of six

seconds. The fluoroscopic images and CAD models were used to create a virtual dual fluoroscopic imaging system (DFIS)[45]. The scapular motions were tracked by matching the glenoid model using radiographic beads implanted in the glenoid fixation pegs from the manufacture to the fluoroscopic images. Similarly, the humeral components were tracked by matching the outlines of their CAD models to the fluoroscopic images. The in-vivo scapular position at each abducted/adducted and rotated position was therefore reproduced using the TSA models. From these models, a coordinate system was placed at the center of the glenoid articular surface and tracked through selected frames of the imaging sequence (Fig 27). The first frame of the sequence served as a normalization for geometric comparison of the scapular motions during the imaging period (Fig 28). The repeatability of reproducing the scapular motion was evaluated by comparing the scapular motion determined by six independent glenoid matches of selected position within the motion cycle.

Results

In-vivo scapular rotation kinematics in 6 DOF after anatomic TSA have been reported relative to a normalized coordinate reference system during a 30° abduction/adduction cycle of the humerus relative to the vertical. Figure 29 shows the rotations about the axes created at the center of the glenoid articular surface. The range being -2° to 23° about the anterior-posterior axis (Y-axis), -11° to 2° about the superior-inferior axis (X-axis), and -8° to 12° about the proximal-distal axis (Z-axis). The repeatability of matching the scapula was found to be 0.1mm in translation and 0.2° in rotation during dynamic motion.

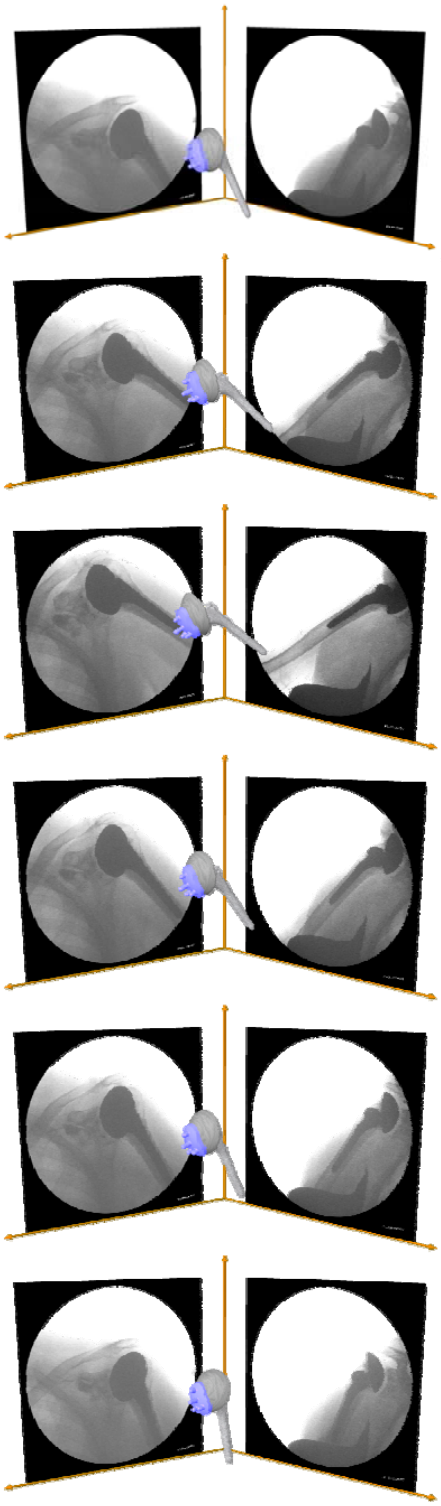

Figure 27 A virtual dual plane fluoroscopic imaging system with TSA components in an abduction / adduction animation sequence. The cycle begins in the top image with a humeral abduction of 28° to the vertical, peaks in the third image at 55° and ends with the bottom image at 23°.

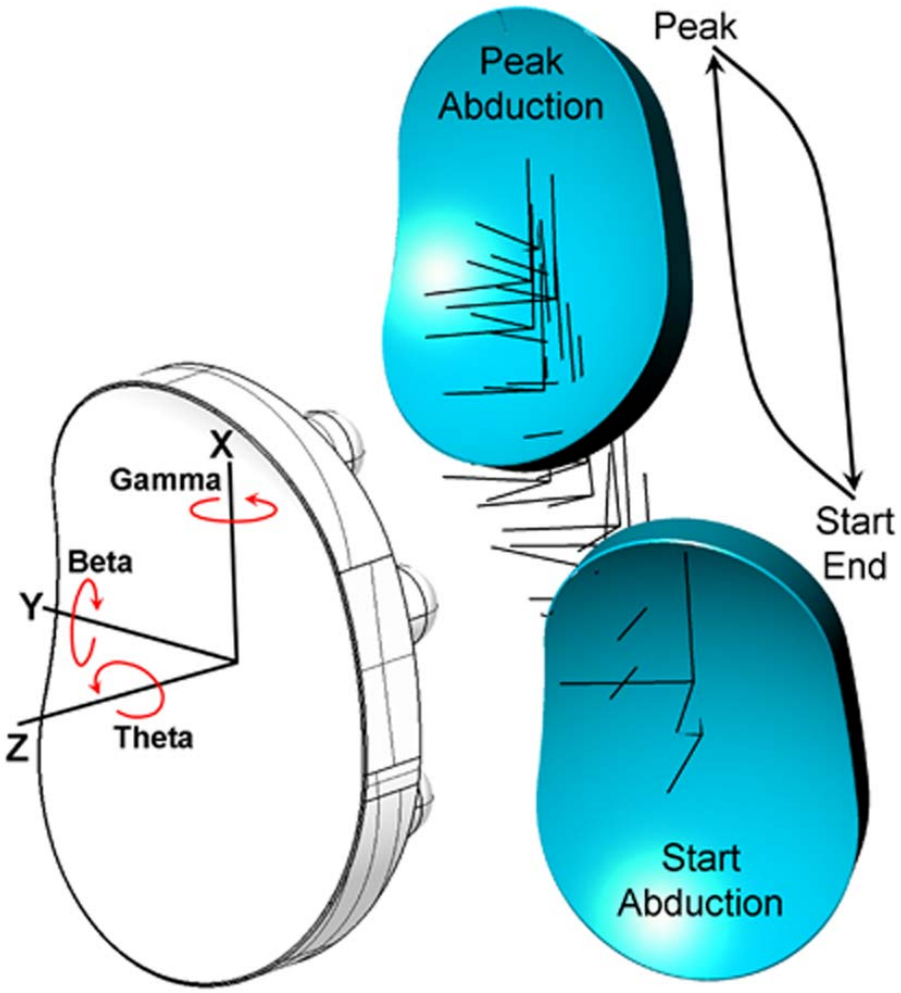

Figure 28 Axes definition of the glenoid with respect to a left shoulder complex shown on the white glenoid. The complex motion path of the glenoid in abduction and adduction over one test cycle is shown by the blue glenoid.

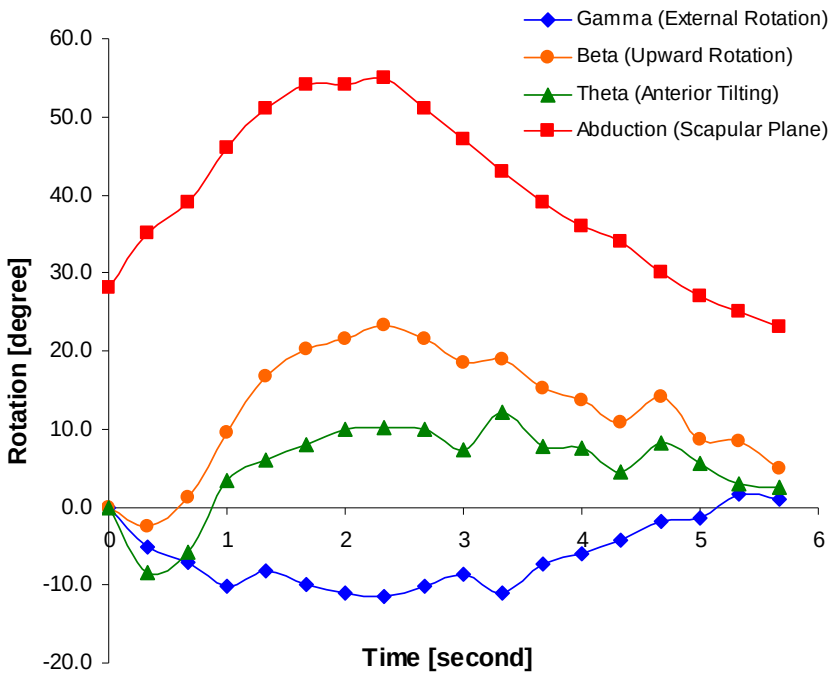

Figure 29 Euler angular rotations of the glenoid normalized to the initial position and humeral abduction / adduction relative to the vertical versus the cycle time. Error bars not shown because they are too small to clearly render.

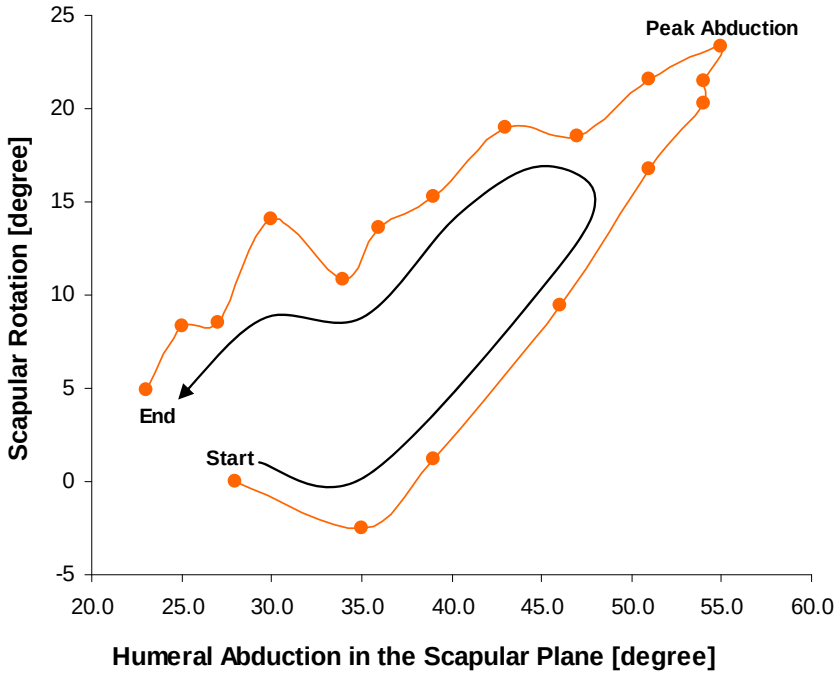

Figure 30 Scapular rotation about the glenoid midline (Y axis) versus abduction / adduction of the humerus relative to the vertical in the plane of the scapula. Hysteresis is exhibited between the transition from abduction to adduction.

Discussion

This work presents the first data on a patient specific gleno-scapular motion after anatomic TSA during a dynamic in-vivo abduction and adduction scapular cycle that simulates daily function. The data indicated that for a humeral abduction of 55° to the vertical, the scapula rotated by about 25° normalized to the initial position, indicating a strong coupling rotation between the humerus and the scapula consistent with the literature[41, 50, 64-66]. Figure 30 shows the relative coupling of the upward and downward rotation of the scapula to the abduction/adduction motion of the humerus during one test cycle. The data indicates that the coupling motion exhibits hysteresis in the transition from the abduction to the adduction phase of arm motion. However, although the patient was told to raise and lower the coffee mug in the same path during the cycle, they were free to choose their own trajectory and could have altered course influencing the amount of hysteresis. Future studies will incorporate a hand rail that the patient will slide their hand along to prevent accidental movement off course. In addition, additional patients will be recruited to build a robust database of scapular motion after anatomic TSA. Nevertheless, these pilot data provide feasibility and repeatability of the systems capability to capture dynamic scapular motion in 6 DOF utilizing a dual fluoroscopic cine imaging technique. These data provide guidelines for future investigation of coupled scapulothoracic kinematics in patients after anatomic TSA and in normal subjects using MRI based bone and cartilage models to investigate glenohumeral contact kinematics during dynamic activities such as pitching a baseball.

4.3.2 Dynamic Shoulder Kinematics - Validation of DFIS

Introduction

Dynamic shoulder kinematics are important for understanding the injury mechanics of the shoulder joint complex and for the improvement of surgical treatment modalities of the injuries. Until recently, little knowledge has been reported on dynamic in-vivo shoulder biomechanics[67, 68]. The purpose of this study was to validate a non-invasive shoulder model based tracking technique to the 'gold standard' marker based technique using a dual plane fluoroscopic imaging system as the shoulder joint was dynamically positioned.

Methods

One male fresh frozen cadaver (age 30) was rigidly fixated to a custom apparatus through pedicle screws in the spinal column that allowed unrestrained motion of the shoulder joint complex (Fig 31). Titanium beads (1/8" diameter) were implanted into the bony surfaces of the humerus and scapula away from the articular cartilage without venting the joint capsule. Fluoroscopic images of the left shoulder were acquired at 30 Hz while the shoulder was manipulated in approximately 150° abduction cycle in the coronal plane. The abduction cycle was performed at approximately 25°/s (slow) and 50°/s (fast), taking six and three seconds respectively to complete. Bone models of the scapula and humerus were constructed using an in-house automated segmentation algorithm from CT scans with a slice thickness of 0.625mm. The fluoroscopic image pairs and bone models of the humerus and scapula were used to create a virtual dual plane fluoroscopic imaging system

(DFIS)[45]. Coordinate systems were placed following the guidelines of the ISB (for a right shoulder joint complex), however axis definitions were rotated 90° to maintain a right-hand coordinate system in the left shoulder joint complex. The humerus and scapula positions were adjusted in six degrees-of-freedom within the virtual system until their projections matched the fluoroscopic images captured during dynamic abduction motion (Fig 32).

Figure 31 Cadaver rigidly mounted to a custom built fixture allowing the shoulder to freely move without obstruction. DFIS shown in image capture geometry.

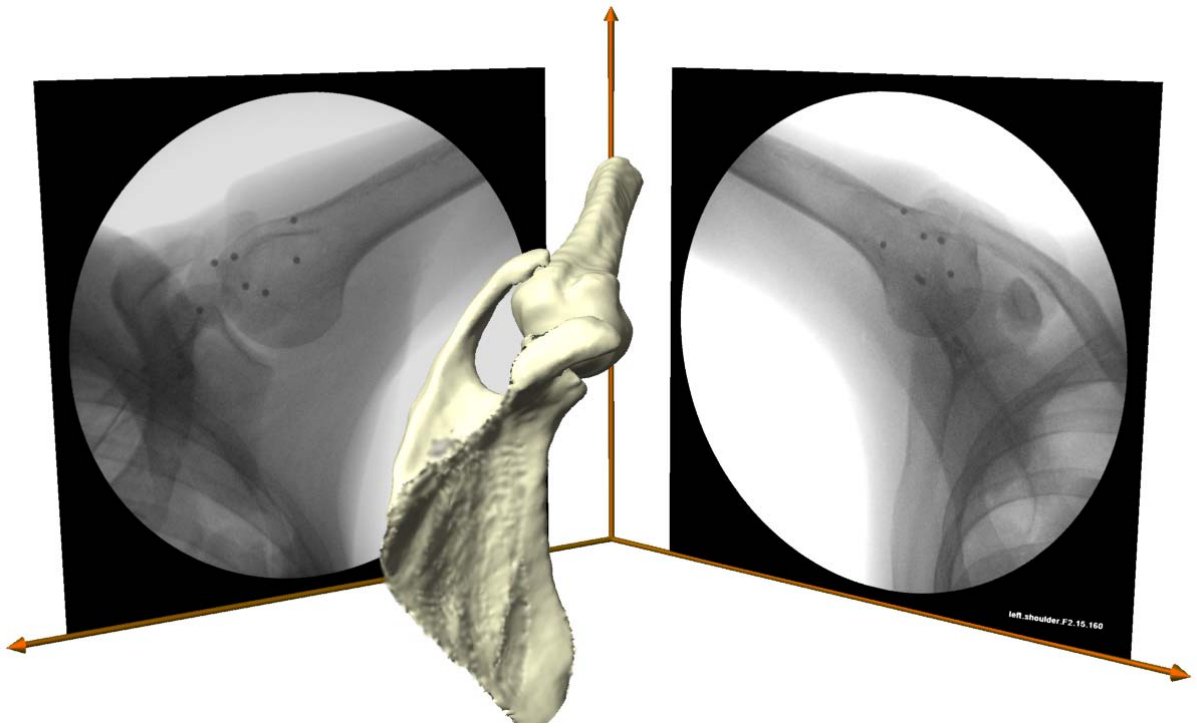

Figure 32 Virtual DFIS created in computer space from the actual geometry of the fluoroscopes shown with 3D model of the scapula and humerus.

This procedure was repeated, but using the implanted titanium beads to align the scapula and humerus. The marker based tracking technique was taken as the 'gold standard' for motion. Ten percent of the acquired fluoroscopic images were analyzed. Translations and rotations of the model based tracking technique were compared to the 'gold standard'. Average error and standard deviation are reported.

Results

Good agreement between model and marker based tracking techniques were observed (Fig 33, 34). Similar errors in translation were observed during fast and slow abduction speeds for both the scapula and humerus (Table 7). However, scapula and humerus rotation errors were almost double during fast abduction compared to slow abduction.

	X (mm)	Y (mm)	Z (mm)	X° (deg)	Y° (deg)	Z° (deg)
Humerus 25°/s	0.25 ± 0.23	0.22 ± 0.16	0.21 ± 0.20	0.33 ± 0.29	0.50 ± 0.21	0.41 ± 0.26
Humerus 50°/s	0.22 ± 0.14	0.29 ± 0.23	0.27 ± 0.20	0.84 ± 0.94	0.76 ± 0.72	0.91 ± 0.96
Scapula 25°/s	0.22 ± 0.13	0.34 ± 0.24	0.26 ± 0.16	0.37 ± 0.22	0.29 ± 0.22	0.40 ± 0.27
Scapula 50°/s	0.34 ± 0.18	0.45 ± 0.12	0.13 ± 0.15	0.78 ± 0.53	0.61 ± 0.63	0.64 ± 0.45

Table 7 Translation and rotation error observed between model and marker 'gold standard' based tracking technique for fast and slow abduction speeds in 6DOF: 3 translations and 3 rotations. Values are reported as Average ± Standard Deviation.

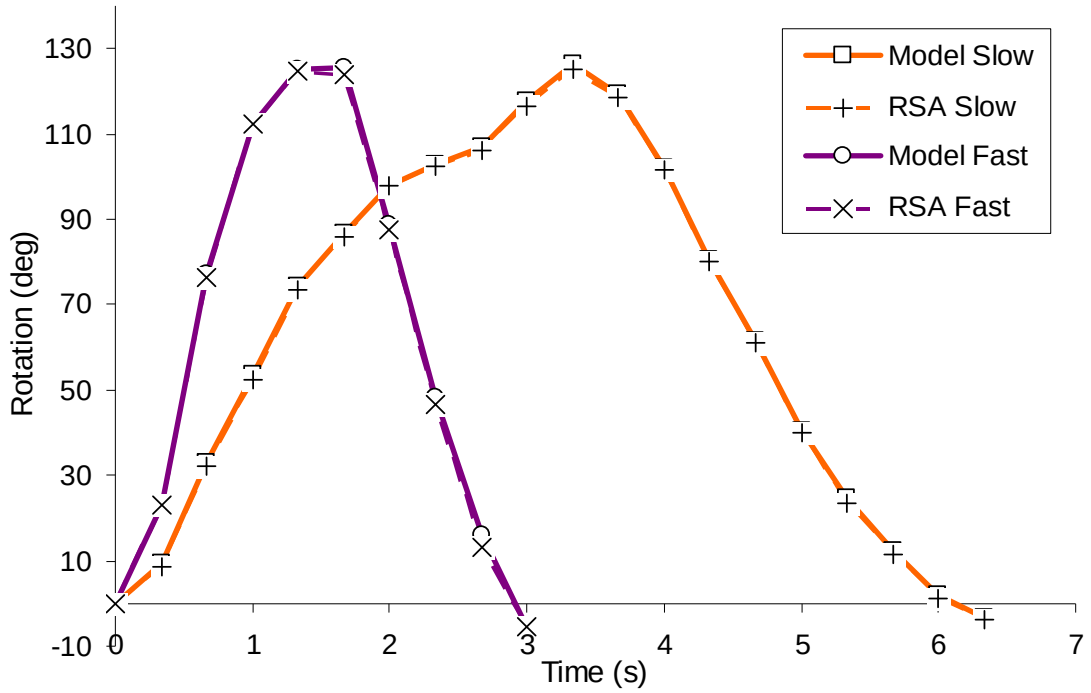

Figure 33 Humerus abduction angle as a function of cycle time. The humerus abduction axis is approximately collinear with the longitudinal axis of the humeral shaft.

Discussion

This work presents the translation and rotation errors of tracking the dynamic motion of the humerus and scapula using a non-invasive model based tracking technique with a dual plane fluoroscopic imaging system. The observed errors in translation and rotation are similar to a validation study of the knee joint using a dual

plane fluoroscopic imaging system[69]. Thus, the data from this study suggests that non-invasive model based tracking could be used to observe in-vivo

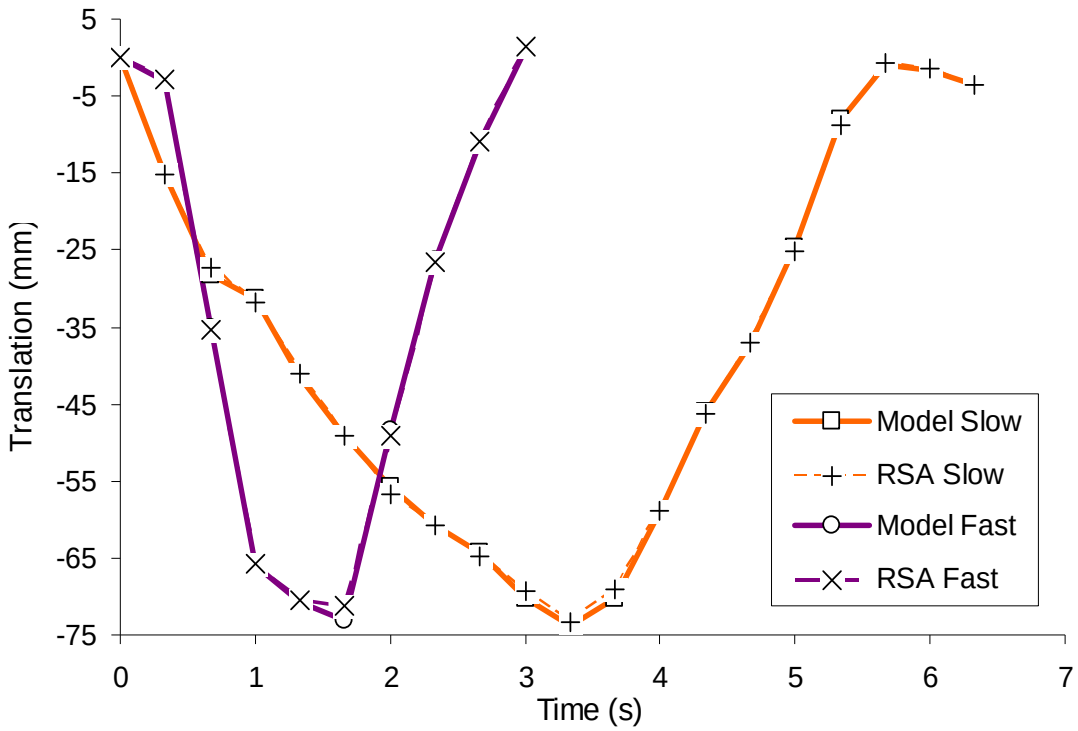

Figure 34 Scapula protraction/retraction translation as a function of cycle time in approximately the coronal plane.

shoulder joint kinematics with similar accuracy as a marker 'gold standard' based tracking technique. This methodology could be useful for measuring the dynamic motion of healthy individuals and in patients with instability.

4.3.3 Mini Grant Proposal For Anterior Stability

Hypothesis

We hypothesize that contemporary reconstructive surgery for anterior shoulder instability does not recreate 'normal' contact patterns of the healthy joint, leading to development of osteoarthritis.

Background and Aims

The shoulder is the most frequently dislocated joint in the human body. It has the greatest range-of-motion of any joint, but the least intrinsic stability (Fig 35). The muscles of the rotator cuff, fibrous cartilage of the glenoid labrum and ligaments of the glenohumeral joint capsule preserve the integrity of the shoulder. Dislocations of the shoulder affect up to 1.7% of the population. It has been estimated that the incidence of all traumatic shoulder dislocations is 11.2 cases per 100,000 persons per year. Approximately 95% of dislocations are anterior; i.e. the translation of the humeral head through the glenohumeral joint capsule anterior to the glenoid fossa. Adults age 18-25 are the most at risk for anterior dislocation due to sports injury. Elderly persons are the second most at risk age population for anterior dislocation due to their susceptibility to falls. Anterior shoulder dislocations usually result from excessive abduction, extension and external rotation, causing the humeral head to be forced out of the glenohumeral joint capsule, rupturing or detaching the anterior capsule from its insertion to the humeral head or from its attachment to the anterior edge of the glenoid fossa. In general, patients complain of excruciating shoulder pain, decreased range-of-motion and an overall reduction in their quality-of-life.

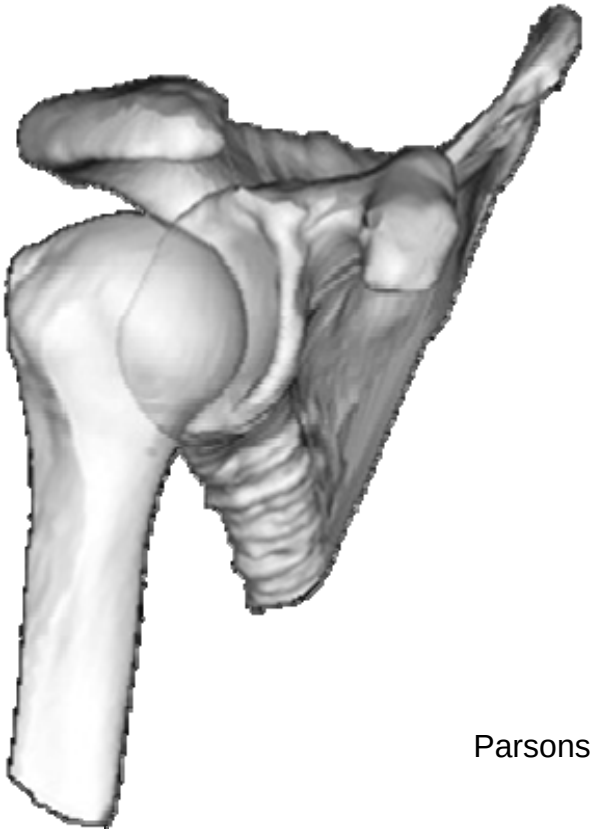

Figure 35 Three dimensional model of the shoulder joint, showing the scapula and humerus bones.

Surgical reconstruction is often performed in an attempt to restore normal stability and decrease pain of the shoulder joint. However, these surgical procedures are known to put patients at significant risk for glenohumeral osteoarthritis, both in the early and late postoperative periods. Early development of postoperative osteoarthritis is associated with improper diagnosis of the instability leading to inadequate surgical treatment or metallic hardware in the joint, even thought clinical stability is restored. However, the underlying causes for later onset of osteoarthritis are unknown. Severe osteoarthritis of the glenohumeral joint is a disabling condition characterized by extreme pain, decreased range-of-motion and overall reduction in

quality-of-life. The surgical treatment for severe osteoarthritis is costly total shoulder joint replacement. The biomechanical factors that affect the onset and development of osteoarthritis after surgical correction for shoulder instability are unknown. Knowledge of these factors may help delay the development of postoperative osteoarthritis after reconstructive surgery for shoulder instability, thus helping to reduce the need for revision instability surgery and costly total shoulder joint replacements.

Recently, a non-invasive imaging technique for analyzing joint kinematics and cartilage contact has been developed at the Bioengineering Laboratory at the Massachusetts General Hospital. The dual plane fluoroscopic imaging system (DFIS)[45] can accurately measure the in-vivo cartilage contact of the glenohumeral joint during daily activities, such as drinking a cup of coffee, throwing a baseball or combing ones hair.

Long-Term Aim

The long-term objective of this project is to identify the biomechanical factors that lead to the onset and development of postoperative osteoarthritis after the surgical treatment for anterior shoulder instability. Patients that have had anterior dislocation and will undergo surgical treatment will be recruited for analysis of their glenohumeral articular contact locations using the DFIS. Preoperative and six months postoperative, the patients will be analyzed for articular contact locations of the affected joint. The patient will again be analyzed at one year and two years postoperative to observe any changes in glenohumeral articular contact patterns.

Short-Term Aim

The short-term objective of this pilot project is to quantify the glenohumeral articular contact locations of the 'normal' shoulder joint in twenty healthy volunteers using the DFIS. This information is vital for the further investigation of shoulder joint behavior following anterior dislocation and subsequent surgery.

Impact

Shoulder instability significantly decreases the quality-of-life in both the young active and elderly populations. This project would quantify for the first time the articular contact locations of the glenohumeral joint. Quantifying the glenohumeral joint articular contact patterns in healthy volunteers and preoperative / postoperative anterior instability patients may help to delineate the biomechanical factors that influence the development of osteoarthritis after surgical treatment for anterior shoulder dislocation. Knowledge of these factors that promote the onset and development of osteoarthritis after surgical intervention for anterior shoulder instability could be used to improve contemporary surgical reconstruction techniques. Improving surgical treatment for anterior shoulder instability may help minimize or delay the onset of osteoarthritis. By minimizing osteoarthritis of the glenohumeral joint, patients would experience a significant decrease in shoulder pain and an increase in range-of-motion. These improvements would reduce the rate of revision instability surgery and delay the need for total shoulder joint replacement.

4.4 Summary

Total shoulder arthroplasty has become the gold standard for restoring ROM and pain relief in degenerative shoulder disease. However, accurate knowledge of in-vivo shoulder kinematics still eludes orthopaedists and researchers. Accurate in-vivo kinematics is the foundation for relative motion between bones, contact patterns of articular surfaces and boundary conditions for finite element and inverse dynamic studies. These data provide orthopaedists and bioengineers a quantitative assessment of normal shoulder motion and the tools which to understand the efficacy that various surgical modalities have on restoring shoulder pathologies. To date, no data has been reported on the glenohumeral joint articular contact locations or humeral head translations in patients following TSA. Contact locations in patients following TSA could be compared to healthy shoulders to determine if normal contact kinematics are restored following surgical reconstruction. Such contact kinematic data are necessary for the improvement of implant designs and surgical implantation technique; and ultimately to enhance component longevity. These data combined with humeral head translations provide in-vivo parameters for wear simulators of the polyethylene glenoid component and a basis which to compare damage modes of failed glenoid components. Thus, quantitatively measuring in-vivo shoulder kinematics would open new doors in the field of shoulder biomechanics. Therefore, the purpose of this research was to investigate the glenohumeral articular contact locations and humeral head translations after anatomic TSA during dynamically stabilized in-vivo shoulder abduction with neutral, internal and external rotations using a novel dual plane fluoroscopic imaging technique.

In conclusion, this study examined the glenohumeral joint articular surface contact kinematics in patients after anatomic TSA that performed active abduction and internal and external rotations of the shoulder. We demonstrated that in-vivo glenohumeral joint contact after TSA was not centered on the glenoid surface, suggesting that anatomic TSA kinematics are not governed by 'ball-in-socket' mechanics as traditionally thought[17, 24, 26-28]. Contact locations as a function of arm position were variable between patients, although in general, contact was favored on the superior-posterior quadrant of the glenoid surface. These data, when compared to normal healthy subjects exhibited similar contact patterns, indicating that anatomic sizing and non-conforming component designs might help better recreate normal kinematics of the glenohumeral joint following primary anatomic TSA.

Appendix A - MATLAB© Files

A.1 circlescentroid.rvb

```
'-----------------------------------------------------------------------------------------
'Created: Daniel Massimini
'Date: July 4, 2006
'Finds closest distance between concave & convex surface

'-----------------------------------------------------------------------------------------

CirclesToSurface 'Name of Function

Sub CirclesToSurface()
Const ObjectSurface = 8 '8 is an identifier for Surface

'-----------------------------------------------------------------------------------------
'Variable Defination & Parameter Specification

Dim HumeralHead, Glenoid, TestPoint(2), UVHumeralHead, UVGlenoid,
NewPointHumeralHead(2), NewPointGlenoid(2)
Dim Count, DummyPoint, MasterIndex
Dim Tolerance, MaxEvaluations, Delta, Index, OldDistance, NewDistance
Dim ClosePointOnHumeralHead, ClosePointOnGlenoid
Dim CircleGlenoid, CircleHumeralHead, LengthGlenoid, LengthHumeralHead
Dim GlenoidCentroid, HumeralHeadCentroid

Tolerance = 0.0000000001
MaxEvaluations = 500
LengthGlenoid = 1

'-----------------------------------------------------------------------------------------
'This Selects the Objects, Humeral Head & Glenoid

HumeralHead = Rhino.GetObject("Please Select the Humeral Head Surface",
ObjectSurface)
If Rhino.IsSurface(HumeralHead) Then

Glenoid = Rhino.GetObject("Please Select Glenoid Surface", ObjectSurface)
If Rhino.IsSurface(Glenoid) Then

'-----------------------------------------------------------------------------------------
'This Picks Three Test Points on the Glenoid
```

```
For Count = 0 To 2 Step 1

  TestPoint(Count) = Rhino.GetPointOnSurface(Glenoid, "Please Pick Test Point "
&Count + 1& " On The Glenoid Surface")
  Dummypoint = TestPoint(Count)
  If IsArray(Dummypoint) Then

End If
Next

'-----------------------------------------------------------------------------------------
'Beginning of Real Loop

MasterIndex = 0

While (LengthGlenoid > 0.2 And MasterIndex < MaxEvaluations)

'-----------------------------------------------------------------------------------------
'This Finds Closest Point to Test Point

For Count = 0 To 2 Step 1

  UVHumeralHead = Rhino.SurfaceClosestPoint(HumeralHead, TestPoint(Count))
  If IsArray(UVHumeralHead) Then
  NewPointHumeralHead(Count) = Rhino.EvaluateSurface(HumeralHead,
UVHumeralHead)

  UVGlenoid = Rhino.SurfaceClosestPoint(Glenoid, NewPointHumeralHead(Count))
  If IsArray(UVGlenoid) Then
  NewPointGlenoid(Count) = Rhino.EvaluateSurface(Glenoid, UVGlenoid)

End If
End If
Next

'-----------------------------------------------------------------------------------------
'This Iterates to Find the Closest Distance

For Count = 0 To 2 Step 1

  Delta = 10 * Tolerance
  Index = 0

  ClosePointOnHumeralHead = NewPointHumeralHead(Count)
  ClosePointOnGlenoid = NewPointGlenoid(Count)
```

```
  While(Delta > Tolerance And Index < MaxEvaluations And
Rhino.IsPointOnSurface(HumeralHead, ClosePointOnHumeralHead) And
Rhino.IsPointOnSurface(Glenoid, ClosePointOnGlenoid))

    OldDistance = Rhino.Distance(ClosePointOnHumeralHead, ClosePointOnGlenoid)

    UVHumeralHead = Rhino.SurfaceClosestPoint(HumeralHead,
ClosePointOnGlenoid)
    If IsArray(UVHumeralHead) Then
    ClosePointOnHumeralHead = Rhino.EvaluateSurface(HumeralHead,
UVHumeralHead)

    UVGlenoid = Rhino.SurfaceClosestPoint(Glenoid, ClosePointOnHumeralHead)
    If IsArray(UVGlenoid) Then
    ClosePointOnGlenoid = Rhino.EvaluateSurface(Glenoid, UVGlenoid)

    NewDistance = Rhino.Distance(ClosePointOnHumeralHead,
ClosePointOnGlenoid)

    Delta = OldDistance - NewDistance
    Index = Index + 1

End If
End If
Wend

NewPointHumeralHead(Count) = ClosePointOnHumeralHead
NewPointGlenoid(Count) = ClosePointOnGlenoid

Next

'-----------------------------------------------------------------------------------------
'This Creates Circles on Humeral Head and Glenoid

CircleHumeralHead =
Rhino.AddCircle3Pt(NewPointHumeralHead(0),NewPointHumeralHead(1),NewPoint
HumeralHead(2))
CircleGlenoid =
Rhino.AddCircle3Pt(NewPointGlenoid(0),NewPointGlenoid(1),NewPointGlenoid(2))

If Rhino.IsCurve(CircleHumeralHead) Then
  LengthHumeralHead = Rhino.CurveLength(CircleHumeralHead)
End If

If Rhino.IsCurve(CircleGlenoid) Then
```

```
  LengthGlenoid = Rhino.CurveLength(CircleGlenoid)
End If

'-------------------------------------------------------------------------------------------
'This Reassigns Variables

For Count = 0 To 2 Step 1

  TestPoint(Count) = NewPointGlenoid(Count)
  Dummypoint = TestPoint(Count)
  If IsArray(Dummypoint) Then
  'Rhino.AddPoint TestPoint(Count)

End If
Next

'-------------------------------------------------------------------------------------------

MasterIndex = MasterIndex + 1

Wend

'End of Loop
'-------------------------------------------------------------------------------------------

If Rhino.IsCurve(CircleGlenoid) Then
  GlenoidCentroid = Rhino.CurveAreaCentroid(CircleGlenoid)
Rhino.AddPoint GlenoidCentroid(0)

If Rhino.IsCurve(CircleHumeralHead) Then
  HumeralHeadCentroid = Rhino.CurveAreaCentroid(CircleHumeralHead)
Rhino.AddPoint HumeralHeadCentroid(0)

NewDistance = Rhino.Distance(GlenoidCentroid(0), HumeralHeadCentroid(0))
Rhino.Print "Distance Between Centroids Is: " & CStr(NewDistance)

End If
End If

Rhino.Print "I Have Completed " & CStr(MasterIndex) & " Iterations!"

End If
End If

End Sub
```

A.2 surfacetocurve.rvb

```
'-------------------------------------------------------------------------------------------
'Created: Daniel Massimini
'Date: July 5, 2006
'Creates curve of surface edge

'May need to modify resulting curves, either removing duplicates or joining sections

'-------------------------------------------------------------------------------------------

SurfaceToCurve

Sub SurfaceToCurve()

Dim Surface

Surface = Rhino.GetObject("Select surface or polysurface (Glenoid Surface)", 24)

If Not IsNull(Surface) Then

Rhino.DuplicateEdgeCurves Surface, True

End If

End Sub
```

A.3 edgetosurface.rvb

```
'-----------------------------------------------------------------------------------------
'Created: Daniel Massimini
'Date: July 5, 2006
'Finds closest distance between curve and surface

'*****************************WARNING*****************************************************

'This script assumes you have a curve of the edge (glenoid) of the surface you want
to test.
'First run surfacetocurve.rvb to create curve, modify and join appropiately.

'-----------------------------------------------------------------------------------------

EdgeToSurface

Sub EdgeToSurface()
'---------------------------------------------------------
Dim HumeralHead, Glenoid, Curve, ArrayPoints, ArrayPoint, UVHumeralHead,
TempPoint
Dim ShortPoint, OldDistance, NewDistance

HumeralHead = Rhino.GetObject("Please Select the Humeral Head Surface", 8)
If Rhino.IsSurface(HumeralHead) Then

Curve = Rhino.GetObject("Select Curve To Measure Closest Point", 4)
If Rhino.IsCurve(Curve) Then

ArrayPoints = Rhino.DivideCurve(Curve, 10000) 'Number of Points

'-------------------------------------------------------------------------
UVHumeralHead = Rhino.SurfaceClosestPoint(HumeralHead, ArrayPoints(0))
If IsArray(UVHumeralHead) Then
TempPoint = Rhino.EvaluateSurface(HumeralHead, UVHumeralHead)

OldDistance = Rhino.Distance(TempPoint, ArrayPoints(0))

'-------------------------------------------------------------------------

For Each ArrayPoint In ArrayPoints


  UVHumeralHead = Rhino.SurfaceClosestPoint(HumeralHead, ArrayPoint)
  If IsArray(UVHumeralHead) Then
```

```
  TempPoint = Rhino.EvaluateSurface(HumeralHead, UVHumeralHead)

  NewDistance = Rhino.Distance(TempPoint, ArrayPoint)

  If (NewDistance < OldDistance) Then
    ShortPoint = ArrayPoint
    OldDistance = NewDistance
  End If

  End If

Next
'-------------------------------------------------------------------------


UVHumeralHead = Rhino.SurfaceClosestPoint(HumeralHead, ShortPoint)
If IsArray(UVHumeralHead) Then
TempPoint = Rhino.EvaluateSurface(HumeralHead, UVHumeralHead)
Rhino.AddPoint ShortPoint
Rhino.AddPoint TempPoint
NewDistance = Rhino.Distance(TempPoint, ShortPoint)
Rhino.Print "Distance Between Points Is: " & CStr(NewDistance)


End If
End If
End If
End If
End Sub
```

References

1. Neer CS, 2nd. Replacement arthroplasty for glenohumeral osteoarthritis. J Bone Joint Surg Am. 1974;56:1-13.

2. Neer CS, Brown TH, Jr., McLaughlin HL. Fracture of the neck of the humerus with dislocation of the head fragment. Am J Surg. 1953;85:252-8.

3. Wirth MA, Rockwood CA, Jr. Complications of total shoulder-replacement arthroplasty. J Bone Joint Surg Am. 1996;78:603-16.

4. Walch G, Edwards TB, Boulahia A, Boileau P, Mole D, Adeleine P. The influence of glenohumeral prosthetic mismatch on glenoid radiolucent lines: results of a multicenter study. J Bone Joint Surg Am. 2002;84-A:2186-91.

5. Roche C, Angibaud L, Flurin PH, Wright T, Zuckerman J. Glenoid loosening in response to dynamic multi-axis eccentric loading: a comparison between keeled and pegged designs with an equivalent radial mismatch. Bull Hosp Jt Dis. 2006;63:88-92.

6. Hopkins AR, Hansen UN, Amis AA, Knight L, Taylor M, Levy O, Copeland SA. Wear in the prosthetic shoulder: association with design parameters. J Biomech Eng. 2007;129:223-30.

7. Hertel R, Ballmer FT. Observations on retrieved glenoid components. J Arthroplasty. 2003;18:361-6.

8. Lo IK, Litchfield RB, Griffin S, Faber K, Patterson SD, Kirkley A. Quality-of-life outcome following hemiarthroplasty or total shoulder arthroplasty in patients with osteoarthritis. A prospective, randomized trial. J Bone Joint Surg Am. 2005;87:2178-85.

9. Hasan SS, Leith JM, Campbell B, Kapil R, Smith KL, Matsen FA, 3rd. Characteristics of unsatisfactory shoulder arthroplasties. J Shoulder Elbow Surg. 2002;11:431-41.

10. Iannotti JP, Gabriel JP, Schneck SL, Evans BG, Misra S. The normal glenohumeral relationships. An anatomical study of one hundred and forty shoulders. J Bone Joint Surg Am. 1992;74:491-500.

11. Soslowsky LJ, Flatow EL, Bigliani LU, Mow VC. Articular geometry of the glenohumeral joint. Clin Orthop. 1992;285:181-90.

12. Kelkar R, Wang VM, Flatow EL, Newton PM, Ateshian GA, Bigliani LU, Pawluk RJ, Mow VC. Glenohumeral mechanics: a study of articular geometry, contact, and kinematics. J Shoulder Elbow Surg. 2001;10:73-84.

13. Terrier A, Buchler P, Farron A. Influence of glenohumeral conformity on glenoid stresses after total shoulder arthroplasty. J Shoulder Elbow Surg. 2006;15:515-20.

14. Lippitt S, Matsen F. Mechanisms of glenohumeral joint stability. Clin Orthop. 1993;291:20-8.

15. Matsen FA, 3rd, Thomas ST: Glenohumeral Instability. In: Surgery of the Musculoskeletal System, pp 1439-1469. Ed by CM Evarts. New York, Churchill Livingstone, 1990

16. Warner JJ, Deng XH, Warren RF, Torzilli PA. Static capsuloligamentous restraints to superior-inferior translation of the glenohumeral joint. Am J Sports Med. 1992;20:675-85.

17. Bigliani LU, Kelkar R, Flatow EL, Pollock RG, Mow VC. Glenohumeral stability. Biomechanical properties of passive and active stabilizers. Clin Orthop Relat Res. 1996;330:13-30.

18. Werner CM, Nyffeler RW, Jacob HA, Gerber C. The effect of capsular tightening on humeral head translations. J Orthop Res. 2004;22:194-201.

19. Wuelker N, Schmotzer H, Thren K, Korell M. Translation of the glenohumeral joint with simulated active elevation. Clin Orthop. 1994;309:193-200.

20. Williams GR, Jr., Wong KL, Pepe MD, Tan V, Silverberg D, Ramsey ML, Karduna A, Iannotti JP. The effect of articular malposition after total shoulder arthroplasty on glenohumeral translations, range of motion, and subacromial impingement. J Shoulder Elbow Surg. 2001;10:399-409.

21. Nyffeler RW, Sheikh R, Atkinson TS, Jacob HA, Favre P, Gerber C. Effects of glenoid component version on humeral head displacement and joint reaction forces: an experimental study. J Shoulder Elbow Surg. 2006;15:625-9.

22. Nyffeler RW, Sheikh R, Jacob HA, Gerber C. Influence of humeral prosthesis height on biomechanics of glenohumeral abduction. An in vitro study. J Bone Joint Surg Am. 2004;86-A:575-80.

23. Harryman DT, 2nd, Sidles JA, Clark JM, McQuade KJ, Gibb TD, Matsen FA, 3rd. Translation of the humeral head on the glenoid with passive glenohumeral motion. J Bone Joint Surg Am. 1990;72:1334-43.

24. Warner JJ, Bowen MK, Deng XH, Hannafin JA, Arnoczky SP, Warren RF. Articular contact patterns of the normal glenohumeral joint. J Shoulder Elbow Surg. 1998;7:381-8.

25. Karduna AR, Williams GR, Williams JL, Iannotti JP. Glenohumeral joint translations before and after total shoulder arthroplasty. A study in cadavera. J Bone Joint Surg Am. 1997;79:1166-74.

26. Howell SM, Galinat BJ, Renzi AJ, Marone PJ. Normal and abnormal mechanics of the glenohumeral joint in the horizontal plane. J Bone Joint Surg Am. 1988;70:227-32.

27. Howell SM, Galinat BJ. The glenoid-labral socket. A constrained articular surface. Clin Orthop. 1989;243:122-5.

28. Poppen NK, Walker PS. Normal and abnormal motion of the shoulder. J Bone Joint Surg Am. 1976;58:195-201.

29. Hopkins AR, Hansen UN, Amis AA, Taylor M, Emery RJ. Glenohumeral kinematics following total shoulder arthroplasty: a finite element investigation. J Orthop Res. 2007;25:108-15.

30. Hopkins AR, Hansen UN, Amis AA, Taylor M, Gronau N, Anglin C. Finite element modelling of glenohumeral kinematics following total shoulder arthroplasty. J Biomech. 2006;39:2476-83.

31. Pfirrmann CW, Huser M, Szekely G, Hodler J, Gerber C. Evaluation of complex joint motion with computer-based analysis of fluoroscopic sequences. Invest Radiol. 2002;37:73-6.

32. Severt R, Thomas BJ, Tsenter MJ, Amstutz HC, Kabo JM. The influence of conformity and constraint on translational forces and frictional torque in total shoulder arthroplasty. Clin Orthop Relat Res. 1993;292:151-8.

33. Wang VM, Krishnan R, Ugwonali OF, Flatow EL, Bigliani LU, Ateshian GA. Biomechanical evaluation of a novel glenoid design in total shoulder arthroplasty. J Shoulder Elbow Surg. 2005;14:129S-140S.

34. Diop A, Maurel N, Grimberg J, Gagey O. Influence of glenohumeral mismatch on bone strains and implant displacements in implanted glenoids. An in vitro experimental study on cadaveric scapulae. J Biomech. 2006;39:3026-35.

35. Stone KD, Grabowski JJ, Cofield RH, Morrey BF, An KN. Stress analyses of glenoid components in total shoulder arthroplasty. J Shoulder Elbow Surg. 1999;8:151-8.

36. Gunther SB, Graham J, Norris TR, Ries MD, Pruitt L. Retrieved glenoid components: a classification system for surface damage analysis. J Arthroplasty. 2002;17:95-100.

37. Weldon EJ, 3rd, Scarlat MM, Lee SB, Matsen FA, 3rd. Intrinsic stability of unused and retrieved polyethylene glenoid components. J Shoulder Elbow Surg. 2001;10:474-81.

38. Bergmann G, Graichen F, Bender A, Kaab M, Rohlmann A, Westerhoff P. In vivo glenohumeral contact forces--measurements in the first patient 7 months postoperatively. J Biomech. 2007;40:2139-49.

39. Nishinaka N, Tsutsui H, Mihara K, Suzuki K, Makiuchi D, Kon Y, Wright TW, Moser MW, Gamada K, Sugimoto H, Banks SA. Determination of in vivo glenohumeral translation using fluoroscopy and shape-matching techniques. J Shoulder Elbow Surg. 2008;17:319-22.

40. Graichen H, Stammberger T, Bonel H, Karl-Hans E, Reiser M, Eckstein F. Glenohumeral translation during active and passive elevation of the shoulder - a 3D open-MRI study. J Biomech. 2000;33:609-13.

41. Bey MJ, Kline SK, Zauel R, Lock TR, Kolowich PA. Measuring dynamic in-vivo glenohumeral joint kinematics: Technique and preliminary results. J Biomech. 2008;41:711-4.

42. Gronenschild E. The accuracy and reproducibility of a global method to correct for geometric image distortion in the x-ray imaging chain. Med Phys. 1997;24:1875-88.

43. Gronenschild E. Correction for geometric image distortion in the x-ray imaging chain: local technique versus global technique. Med Phys. 1999;26:2602-16.

44. Canny J. A computational approach to edge detection IEEE Trans. Pattern Anal. Mach. Intell. . 1986 8 679-698

45. Li G, Wuerz TH, DeFrate LE. Feasibility of using orthogonal fluoroscopic images to measure in vivo joint kinematics. J Biomech Eng. 2004;126:314-8.

46. Stormont TJ, An KN, Morrey BF, Chao EY. Elbow joint contact study: comparison of techniques. J Biomech. 1985;18:329-36.

47. Wan L, de Asla RJ, Rubash HE, Li G. Determination of in-vivo articular cartilage contact areas of human talocrural joint under weightbearing conditions. Osteoarthritis Cartilage. 2006;14:1294-301.

48. Inman VT, Saunders JB, Abbott LC. Observations on the function of the shoulder joint. J Bone Joint Surg Am. 1944;26:1-30.

49. McQuade KJ, Smidt GL. Dynamic scapulohumeral rhythm: the effects of external resistance during elevation of the arm in the scapular plane. J Orthop Sports Phys Ther. 1998;27:125-33.

50. Freedman L, Munro RR. Abduction of the arm in the scapular plane: scapular and glenohumeral movements. A roentgenographic study. J Bone Joint Surg Am. 1966;48:1503-10.

51. Crosbie J, Kilbreath SL, Hollmann L, York S. Scapulohumeral rhythm and associated spinal motion. Clin Biomech (Bristol, Avon). 2008;23:184-92.

52. Gupta R, Lee TQ. Positional-dependent changes in glenohumeral joint contact pressure and force: possible biomechanical etiology of posterior glenoid wear. J Shoulder Elbow Surg. 2005;14:105S-110S.

53. Apreleva M, Parsons IMt, Warner JJ, Fu FH, Woo SL. Experimental investigation of reaction forces at the glenohumeral joint during active abduction. J Shoulder Elbow Surg. 2000;9:409-17.

54. Anglin C, Wyss UP, Pichora DR. Glenohumeral contact forces. Proc Inst Mech Eng [H]. 2000;214:637-44.

55. Poppen NK, Walker PS. Forces at the glenohumeral joint in abduction. Clin Orthop. 1978;135:165-70.

56. van der Helm FC, Pronk GM. Three-dimensional recording and description of motions of the shoulder mechanism. J Biomech Eng. 1995;117:27-40.

57. Conzen A, Eckstein F. Quantitative determination of articular pressure in the human shoulder joint. J Shoulder Elbow Surg. 2000;9:196-204.

58. Soslowsky LJ, Flatow EL, Bigliani LU, Pawluk RJ, Ateshian GA, Mow VC. Quantitation of in situ contact areas at the glenohumeral joint: a biomechanical study. J Orthop Res. 1992;10:524-34.

59. Boyer PJ, Massimini DF, Gill TJ, Papannagari R, Stewart SL, Warner JP, Li G. In vivo articular cartilage contact at the glenohumeral joint: preliminary report. J Orthop Sci. 2008;13:359-65.

60. Karduna AR, Williams GR, Iannotti JP, Williams JL. Total shoulder arthroplasty biomechanics: a study of the forces and strains at the glenoid component. J Biomech Eng. 1998;120:92-9.

61. Rhoad RC, Klimkiewicz JJ, Williams GR, Kesmodel SB, Udupa JK, Kneeland JB, Iannotti JP. A new in vivo technique for three-dimensional shoulder kinematics analysis. Skeletal Radiol. 1998;27:92-7.

62. Schiffern SC, Rozencwaig R, Antoniou J, Richardson ML, Matsen FA, 3rd. Anteroposterior centering of the humeral head on the glenoid in vivo. Am J Sports Med. 2002;30:382-7.

63. Walch G, Boileau P. Prosthetic adaptability: a new concept for shoulder arthroplasty. J Shoulder Elbow Surg. 1999;8:443-51.

64. Berthonnaud E, Herzberg G, Zhao KD, An KN, Dimnet J. Three-dimensional in vivo displacements of the shoulder complex from biplanar radiography. Surg Radiol Anat. 2005;27:214-22.

65. Borstad JD, Ludewig PM. Comparison of scapular kinematics between elevation and lowering of the arm in the scapular plane. Clin Biomech (Bristol, Avon). 2002;17:650-9.

66. Ebaugh DD, McClure PW, Karduna AR. Three-dimensional scapulothoracic motion during active and passive arm elevation. Clin Biomech (Bristol, Avon). 2005;20:700-9.

67. Bey MJ, Zauel R, Brock SK, Tashman S. Validation of a new model-based tracking technique for measuring three-dimensional, in vivo glenohumeral joint kinematics. J Biomech Eng. 2006;128:604-9.

68. McClure PW, Michener LA, Sennett BJ, Karduna AR. Direct 3-dimensional measurement of scapular kinematics during dynamic movements in vivo. J Shoulder Elbow Surg. 2001;10:269-77.

69. Li G, Wan L, Kozanek M. Determination of real-time in-vivo cartilage contact deformation in the ankle joint. J Biomech. 2008;41:128-36.